1-1-2010

Scaled Momentum Spectra in Deep Inelastic Scattering at HERA

H. Abramowicz
Tel Aviv University

I. Abt
Max Planck Institute for Physics (Werner Heisenberg Institute)

L. Adamczyk
AGH University of Science and Technology

M. Adamus
Institute of Nuclear Chemistry and Technology, Warsaw

S. Antonelli
Istituto Nazionale di Fisica Nucleare, Sezione di Bologna

See next page for additional authors

Published for SISSA by Springer

Received: *January 27, 2010*
Accepted: *April 27, 2010*
Published: *June 3, 2010*

Scaled momentum spectra in deep inelastic scattering at HERA

ZEUS collaboration

E-mail: tobias.haas@desy.de

Abstract: Charged particle production has been studied in neutral current deep inelastic ep scattering with the ZEUS detector at HERA using an integrated luminosity of $0.44\,\mathrm{fb}^{-1}$. Distributions of scaled momenta in the Breit frame are presented for particles in the current fragmentation region. The evolution of these spectra with the photon virtuality, Q^2, is described in the kinematic region $10 < Q^2 < 41000\,\mathrm{GeV}^2$. Next-to-leading-order and modified leading-log-approximation QCD calculations as well as predictions from Monte Carlo models are compared to the data. The results are also compared to e^+e^- annihilation data. The dependences of the pseudorapidity distribution of the particles on Q^2 and on the energy in the γp system, W, are presented and interpreted in the context of the hypothesis of limiting fragmentation.

Keywords: Lepton-Nucleon Scattering

ArXiv ePrint: 1001.4026v1

doi:10.1007/JHEP06(2010)009

JHEP06(2010)009

Contents

JHEP06(2010)009

1 Introduction

Quark fragmentation has previously been studied experimentally in deep inelastic ep scattering (DIS) at HERA using observables such as multiplicity moments, scaled momentum distributions and fragmentation functions [1–4]. The results were compared to those obtained in e^+e^- and $p\overline{p}$ collisions. In general, universal behaviour has been established and scaling violations of the fragmentation functions [5, 6] observed. It has also been observed that perturbative Quantum Chromodynamics (pQCD) calculations using the modified leading-log-approximation (MLLA) [7–10] and assuming local parton-hadron duality (LPHD) [11] do not provide a full description of the data.

In this paper, multiplicity distributions of charged hadrons in the current region in the Breit frame[1] are presented as functions of the virtuality of the exchanged boson, Q^2 per unit of the scaled momentum, $x_p = 2P_{\mathrm{Breit}}/Q$, and the variable $\ln(1/x_p)$ in bins of Q^2. Here, P_{Breit} denotes the momentum of a hadron in the Breit frame. The data sample collected with the ZEUS detector between 1996–2007, comprising $0.44\,\mathrm{fb}^{-1}$, enables the study to be extended to Q^2 as high as $41\,000\ \mathrm{GeV}^2$. Predictions from next-to-leading-order (NLO) QCD calculations that combine full NLO matrix elements with fragmentation functions (FF) obtained from fits to e^+e^- annihilation data [12–17] are compared to the measurements. Predictions from MLLA+LPHD [10, 18, 19] and leading-order plus parton-shower Monte Carlo programs are also considered.

[1] The Breit frame is defined as the frame in which the four-vector of the exchanged photon becomes (0,0,0,-Q).

In addition, the measurements are compared to previous ep results [1–4] and to e^+e^- annihilation data [20–23]. The hadronisation in the current region in the Breit frame in ep scattering can be compared directly to the hadronisation in one hemisphere of e^+e^- annihilation events. There, particle momenta are scaled to half of the centre-of-mass energy, $E^* = \sqrt{s}/2$. Previous studies on DIS hadronisation [1–4, 24] have shown good agreement with e^+e^- annihilation at medium Q^2. At lower Q^2, $Q^2 < 40\,\mathrm{GeV}^2$, the two processes were observed to behave differently [3]. This can be explained by higher-order QCD processes such as boson-gluon fusion (BGF) and initial-state QCD Compton radiation occurring as part of the hard interaction in ep scattering but not in e^+e^- annihilation.

Finally, the density of charged particles is studied as a function of the particle pseudo-rapidity, η^{Breit}, in bins of Q^2, and as a function of the total $\gamma^\star p$ centre-of-mass energy, W. The data are used to test the hypothesis of limiting fragmentation [25], in which there has recently been renewed interest, most notably in relativistic heavy ion collisions [26–30].

2 Experimental setup

A detailed description of the ZEUS detector can be found elsewhere [31]. A brief outline of the components most relevant for this analysis is given below. Charged particles were tracked in the central tracking detector (CTD) [32–34], which operated in a magnetic field of 1.43 T provided by a thin superconducting solenoid. The CTD consisted of 72 cylindrical drift-chamber layers, organized in nine superlayers covering the polar-angle[2] region $15° < \theta < 164°$ and the radial range from 18.2 cm to 79.4 cm. Before the 2003–2007 running period, the ZEUS tracking system was upgraded with a silicon microvertex detector (MVD) [35].

The high-resolution uranium-scintillator calorimeter (CAL) [36–39] covered 99.7% of the total solid angle and consisted of three parts: the forward (FCAL), the barrel (BCAL) and the rear (RCAL) calorimeters. Each part was subdivided transversely into towers and longitudinally into one electromagnetic section (EMC) and either one (in RCAL) or two (in BCAL and FCAL) hadronic sections (HAC). The smallest subdivision of the CAL was called a cell. Under test-beam conditions, the CAL single-particle relative energy resolutions were $\sigma_E/E = 0.18/\sqrt{E}$ for electrons and $\sigma_E/E = 0.35/\sqrt{E}$ for hadrons, with E in GeV.

The position of the scattered electron was determined by combining information from the CAL, the small-angle rear tracking detector (SRTD) [40] and the presampler (PRES) [41], both mounted on the face of the RCAL.

The luminosity was measured using the Bethe-Heitler process $ep \to e\gamma p$ by a luminosity detector which consisted of a lead-scintillator [42–44] calorimeter and, after 2002, an independent magnetic spectrometer [45]. The fractional systematic uncertainty on the measured luminosity was 2% and 2.6% for the 1996–2000 and 2004–2007 running periods, respectively.

[2] The ZEUS coordinate system is a right-handed Cartesian system, with the Z axis pointing in the proton beam direction, referred to as the "forward direction", and the X axis pointing towards the centre of HERA. The coordinate origin is at the nominal interaction point.

JHEP06(2010)009

$Q^2_{\rm DA}$ (GeV^2)	scaled momenta		limiting fragmentation	
	$x_{\rm DA}$	no. of events	W (GeV)	no. of events
10 – 30	—	—	80 – 160	1 142 102
30 – 160	—	—	80 – 200	1 185 843
160 – 320	0.0024 – 0.0500	684 077	80 – 240	584 578
320 – 640	0.0100 – 0.0500	170 784	120 – 240	152 367
640 – 1280		72 268	120 – 280	75 176
1280 – 2560	0.025 – 0.15	31 608	120 – 280	29 949
2560 – 5120	0.05 – 0.25	10 858	160 – 280	8 031
5120 – 10240	0.05 – 0.50	4 748	160 – 280	2 914
10240 – 20480		1 197	—	—
20480 – 40960	0.05 – 0.75	205	—	—

Table 1. Number of accepted events in (Q^2,x) bins for the scaled momentum analysis and in (W,Q^2) bins for limiting-fragmentation studies.

3 Event sample

The data presented here were collected with the ZEUS detector at HERA between 1996 and 2007 and correspond to an integrated luminosity of $0.44\,\mathrm{fb}^{-1}$. During 1995–97 (1998-2007) HERA operated with protons with an energy of $E_p = 820$ GeV (920 GeV) and electrons[3] with an energy of $E_e = 27.5$ GeV, resulting in a centre-of-mass energy of $\sqrt{s} = 300$ GeV (318 GeV).

A three-level trigger system [31, 46, 47] was used to select events online. It relied on the presence of an energy deposition in the CAL compatible with that of a scattered electron. At the third level, an electron, identified using the pattern of energy deposits in the CAL [48] and having an energy larger than 4 GeV, was required.

The kinematic variables, Q^2 and the Bjorken scaling variable, x, as well as the boost vector to the Breit frame were reconstructed using the double angle (DA) method [49] based on the angles of the scattered electron and of the hadronic system. The total energy of the γp-system, W, was calculated using $W^2 = Q^2_{\rm DA}(1 - x_{\rm DA})/x_{\rm DA}$.

The tracks used in the analysis had to be associated with the primary interaction vertex and were required to be in the region of high CTD acceptance, $|\eta| < 1.75$, where $\eta = -\ln(\tan\theta/2)$ is the pseudorapidity of the track in the laboratory frame with θ being the polar angle of the measured track with respect to the proton direction. The tracks had to pass through at least three CTD superlayers and were required to have a transverse momentum, $P_T^{\rm track} > 150$ MeV. The details of the event reconstruction are similar to those in a previous ZEUS publication [3] and are described in detail elsewhere [50].

[3]The term "electron" is used for both electrons and positrons.

JHEP06(2010)009

To reconstruct x_p, the momentum four-vector of each track was boosted to the Breit frame assuming the particle to have the pion mass.

The analysis of the scaled momenta was restricted to events with $Q^2 > 160\,\mathrm{GeV}^2$. A well reconstructed neutral current DIS sample was selected by requiring the following:

- $E'_e > 10\,\mathrm{GeV}$, where E'_e is the energy of the scattered electron;
- $y_e \leq 0.95$, where y_e is the inelasticity, $y = Q^2/sx$, estimated from the energy and angle of the scattered electron; this reduces the photoproduction background;
- $y_{\mathrm{JB}} \geq 0.04$, where y_{JB} is estimated by the Jacquet-Blondel method [51]; this rejects events for which the DA method gives a poor reconstruction;
- $35 \leq \delta \leq 60\,\mathrm{GeV}$, where $\delta = \sum(E_i - P_{Z_i})$ and E_i is the energy of the i-th calorimeter cell, P_{Z_i} is its momentum along the Z axis and the sum runs over all cells; this removes photoproduction and events with initial-state radiation;
- $|Z_{\mathrm{vertex}}| < 50$ cm, where Z_{vertex} is the Z component of the position of the primary interaction vertex; this reduces background from events not originating from ep collisions;
- the position (X, Y) of the scattered electron candidates in the RCAL was required to satisfy $\sqrt{X^2 + Y^2} > 35$ cm.

The limiting-fragmentation analysis was extended to events with lower Q^2 values, $Q^2 > 10\,\mathrm{GeV}^2$, using data collected during 1996–2000 corresponding to an integrated luminosity of 77 pb^{-1}. The same selection as described above was used but, for events with $10 < Q^2 < 160\ \mathrm{GeV}^2$, the last requirement was modified and one additional requirement introduced:

- depending on experimental conditions, the position (X, Y) of the scattered electron candidate in the RCAL was required to satisfy $|X| > 12$ cm and $|Y| > 6$ cm or $|X| > 14$ cm and $|Y| > 14$ cm or $\sqrt{X^2 + Y^2} > 35$ cm.
- $\eta_{\mathrm{max}} > 3.2$, where η_{max} is the pseudorapidity in the laboratory frame of the most forward energy deposit with at least 400 MeV; this removes diffractive events. Even before the cut, for $Q^2 > 100\,\mathrm{GeV}^2$, the contamination with diffractive events is well below 5 %, and the resulting corrections to the multiplicity are below 2 %. In the lowest Q^2 bin, the contribution of diffractive events would grow up to 10 % without the cut.

Only tracks with $P_Z^{\mathrm{Breit}} < 0$ enter the analysis of the scaled momenta, whereas this restriction does not apply to the limiting-fragmentation studies. The total number of events is listed in table 1.

4 Models and Monte Carlo simulations

The NLO perturbative QCD calculations considered, combine the full NLO matrix elements with NLO fragmentation functions obtained from fits to e^+e^- data [12–17]. The resulting predictions were obtained using the CYCLOPS program [52].

JHEP06(2010)009

The MLLA calculations [10, 18, 53–55] describe parton production in terms of a shower evolution. They depend on two parameters only, the effective QCD scale, $\Lambda_{\rm eff}$, and the infrared cutoff scale, Q_0, at which the parton cascade is stopped. The calculations intrinsically include colour coherence and gluon interference effects. Leading collinear and infrared singularities are removed and energy-momentum conservation is obeyed.

To connect predictions at the parton level to the hadron-level data, LPHD [11] was assumed, which leaves only one free parameter, the hadronisation constant, K_h. The conversion from energy to momentum spectra for the final-state hadrons was performed assuming an effective hadron mass, $m_{\rm eff} = Q_0$ [19]. The input parameters for the calculations were obtained by fits to LEP e^+e^- data. Conservative uncertainties, equivalent to three standard deviations of the experimental uncertainty, were assumed for the parameters: $Q_0 = \Lambda_{\rm eff} = 270 \pm 20\,\text{MeV}$ and $K_h = 1.31 \pm 0.03$. The $\Lambda_{\rm eff}$ value agrees with the value $\Lambda_{\rm eff} = 275 \pm 4(\text{stat.})^{+4}_{-8}(\text{syst.})\,\text{MeV}$ deduced from a ZEUS analysis of scaled momenta in dijet photoproduction [56]. The usage of input parameters deduced from LEP data is justified by the assumed equivalence of hadronisation in one hemisphere of e^+e^- annihilation and in the current region of ep interactions in the Breit frame.

The predictions from several Monte Carlo (MC) models were compared to the measurements. Neutral current DIS events were generated using the leading-order QCD ARIADNE 4.12 program [57]. The QCD cascade was simulated using the colour-dipole model (CDM) [58] inside ARIADNE. Additional samples were generated with the MEPS model of LEPTO 6.5 [59]. Both MC programs, ARIADNE and LEPTO, were also used to calculate detector acceptances and to correct the data to the hadron level. For this purpose,they were used with the DJANGOH 1.1 [60] interface and QED radiative effects are included using the HERACLES 4.6.1 [61] program. Both MC programs use the Lund string model [62] for hadronisation as implemented in JETSET 7.4 [63, 64]. Hadrons are assumed stable if their lifetime is larger than 3×10^{-11} s; their decay products are not considered. This excludes in particular the charged decay products of K^0 and Λ particles.

All generated events were passed through the ZEUS detector- and trigger-simulation programs which are based on GEANT 3 [65]. They were reconstructed and analysed by the same program chain as the data.

5 Correction procedure and systematic uncertainties

All measured distributions were corrected to the hadron level. The correction factors were calculated bin by bin using MC events. For the scaled momentum spectra, the factors are typically below 1.2 for $Q^2 < 5000\ \text{GeV}^2$, but rise up to 1.5 for higher Q^2. The corrections for charged-particle densities as a function of the pseudorapidity are of a similar magnitude and approach 1.5 as $\eta^{\rm Breit}$ increases towards the most positive values measured.

Cross sections, measured separately for each data-taking period, were combined using a standard weighted average [66]. The dependence of the scaled momentum distributions on the variation of the proton-beam energy in the different data samples was determined using MC events; the resulting changes were found to be smaller than 0.5% and were neglected.

JHEP06(2010)009

Finally, the results were corrected to the QED Born level using correction factors obtained from MC, reducing the charged hadron multiplicities by up to 4%.

The systematic uncertainties were investigated separately for data with Q^2 above and below 160 GeV^2. The numbers in parentheses correspond to the largest variations observed in the scaled momentum spectra. The uncertainties in the limiting-fragmentation distributions are of similar magnitude. For data with $Q^2 > 160$ GeV^2, the systematic uncertainties are due to:

- imperfections in the simulation affecting the determination of the efficiency of event reconstruction and event selection ($^{+1}_{-2}$%). This was evaluated by modifying the selection cuts within the experimental resolutions.
- an uncertainty of 3% in the overall tracking efficiency (± 3%).
- track reconstruction uncertainties close to the borders of acceptance ($^{+6}_{-3}$%). This was evaluated by
  - raising (lowering) the cut on P_T^{track} to 160 MeV (140 MeV);
  - requiring $|\eta| < 1.5$ instead of 1.75; this effect dominates for $Q^2 > 10000\,\mathrm{GeV}^2$;
  - including tracks not associated to the primary vertex.
- alignment uncertainties affecting the calculation of the boost vector to the Breit frame ($^{+3}_{-2}$%). This was evaluated by
  - varying the polar angle for the scattered electron by ± 2 mrad;
  - varying the polar angles for the hadrons by ± 4 mrad.
- assumptions concerning the details of the simulation of the hadronic final state (-4%). This was estimated by using LEPTO instead of ARIADNE.

For data with $Q^2 < 160$ GeV^2, the systematic uncertainties are slightly different and are due to:

- imperfections in the simulation affecting the determination of the efficiency of event reconstruction and event selection ($^{+3}_{-1}$%).
- track reconstruction uncertainties ($^{+5}_{-0.5}$%).
- assumptions concerning the details of the simulation of the hadronic final state ($+7$%).
- an uncertainty about the size of the contribution of diffractive events ($^{+2}_{-1}$%). This was estimated by varying the η_{max} cut by ± 0.2 units.

Further details can be found elsewhere [50]. All individual uncertainties were added in quadrature.

JHEP06(2010)009

$\ln(1/x_p)$	$160 < Q^2 < 320\,\mathrm{GeV}^2$	$320 < Q^2 < 640\,\mathrm{GeV}^2$
0.00–0.25	$0.0319 \pm 0.0005^{+0.0011}_{-0.0012}$	$0.0259 \pm 0.0009^{+0.0009}_{-0.0010}$
0.25–0.50	$0.1156 \pm 0.0011^{+0.0041}_{-0.0039}$	$0.101 \pm 0.002^{+0.003}_{-0.004}$
0.50–0.75	$0.2573 \pm 0.0016^{+0.0079}_{-0.0079}$	$0.232 \pm 0.003^{+0.010}_{-0.007}$
0.75–1.00	$0.451 \pm 0.002^{+0.014}_{-0.014}$	$0.419 \pm 0.004^{+0.015}_{-0.012}$
1.00–1.25	$0.695 \pm 0.003^{+0.022}_{-0.021}$	$0.654 \pm 0.005^{+0.026}_{-0.019}$
1.25–1.50	$0.959 \pm 0.003^{+0.030}_{-0.028}$	$0.925 \pm 0.006^{+0.031}_{-0.026}$
1.50–1.75	$1.216 \pm 0.004^{+0.039}_{-0.037}$	$1.191 \pm 0.007^{+0.039}_{-0.034}$
1.75–2.00	$1.437 \pm 0.004^{+0.044}_{-0.044}$	$1.440 \pm 0.008^{+0.044}_{-0.044}$
2.00–2.25	$1.587 \pm 0.004^{+0.051}_{-0.049}$	$1.658 \pm 0.008^{+0.054}_{-0.047}$
2.25–2.50	$1.643 \pm 0.004^{+0.051}_{-0.051}$	$1.772 \pm 0.008^{+0.056}_{-0.051}$
2.50–2.75	$1.599 \pm 0.004^{+0.050}_{-0.049}$	$1.861 \pm 0.008^{+0.056}_{-0.053}$
2.75–3.00	$1.459 \pm 0.004^{+0.049}_{-0.044}$	$1.829 \pm 0.008^{+0.055}_{-0.053}$
3.00–3.25	$1.215 \pm 0.003^{+0.038}_{-0.038}$	$1.673 \pm 0.008^{+0.056}_{-0.049}$
3.25–3.50	$0.927 \pm 0.003^{+0.028}_{-0.036}$	$1.398 \pm 0.007^{+0.043}_{-0.042}$
3.50–3.75	$0.649 \pm 0.002^{+0.021}_{-0.036}$	$1.087 \pm 0.006^{+0.033}_{-0.033}$
3.75–4.00	$0.4209 \pm 0.0019^{+0.0127}_{-0.0277}$	$0.778 \pm 0.005^{+0.026}_{-0.028}$
4.00–4.25	$0.2561 \pm 0.0015^{+0.0078}_{-0.0219}$	$0.517 \pm 0.004^{+0.018}_{-0.025}$
4.25–4.50	$0.1473 \pm 0.0011^{+0.0047}_{-0.0141}$	$0.317 \pm 0.003^{+0.010}_{-0.017}$
4.50–4.75	$0.0842 \pm 0.0009^{+0.0032}_{-0.0081}$	$0.184 \pm 0.002^{+0.006}_{-0.013}$
4.75–5.00	$0.0474 \pm 0.0007^{+0.0016}_{-0.0045}$	$0.1079 \pm 0.0019^{+0.0032}_{-0.0061}$
5.00–5.25	$0.0266 \pm 0.0006^{+0.0008}_{-0.0022}$	$0.0598 \pm 0.0015^{+0.0024}_{-0.0046}$
5.25–5.50	$0.0167 \pm 0.0006^{+0.0007}_{-0.0025}$	$0.0356 \pm 0.0013^{+0.0011}_{-0.0021}$
5.50–5.75	$0.0102 \pm 0.0006^{+0.0014}_{-0.0017}$	$0.0208 \pm 0.0012^{+0.0011}_{-0.0019}$
5.75–6.00	$0.0069 \pm 0.0008^{+0.0008}_{-0.0040}$	$0.0126 \pm 0.0012^{+0.0011}_{-0.0041}$
6.00–6.25	$0.0040 \pm 0.0011^{+0.0015}_{-0.0051}$	$0.0092 \pm 0.0016^{+0.0033}_{-0.0012}$
6.25–6.50	$0.008 \pm 0.007^{+0.002}_{-0.004}$	$0.004 \pm 0.002^{+0.031}_{-0.008}$

Table 2. The bin-averaged scaled momentum spectra, $1/N\ dn^{\pm}/d\ln(1/x_p)$, for $160 < Q^2 < 640\,\mathrm{GeV}^2$. The first uncertainty is statistical, the second systematic.

JHEP06(2010)009

$\ln(1/x_p)$	$640 < Q^2 < 1280\,\mathrm{GeV}^2$	$1280 < Q^2 < 2560\,\mathrm{GeV}^2$
0.00–0.25	$0.0228 \pm 0.0013^{+0.0017}_{-0.0014}$	$0.0236 \pm 0.0016^{+0.0014}_{-0.0013}$
0.25–0.50	$0.086 \pm 0.003^{+0.006}_{-0.006}$	$0.087 \pm 0.004^{+0.003}_{-0.004}$
0.50–0.75	$0.218 \pm 0.004^{+0.007}_{-0.011}$	$0.199 \pm 0.006^{+0.011}_{-0.006}$
0.75–1.00	$0.371 \pm 0.006^{+0.013}_{-0.011}$	$0.368 \pm 0.009^{+0.023}_{-0.011}$
1.00–1.25	$0.597 \pm 0.007^{+0.018}_{-0.022}$	$0.577 \pm 0.011^{+0.032}_{-0.016}$
1.25–1.50	$0.857 \pm 0.009^{+0.027}_{-0.031}$	$0.840 \pm 0.014^{+0.035}_{-0.024}$
1.50–1.75	$1.121 \pm 0.010^{+0.034}_{-0.037}$	$1.098 \pm 0.015^{+0.039}_{-0.032}$
1.75–2.00	$1.346 \pm 0.011^{+0.041}_{-0.044}$	$1.325 \pm 0.017^{+0.052}_{-0.039}$
2.00–2.25	$1.598 \pm 0.012^{+0.048}_{-0.050}$	$1.535 \pm 0.017^{+0.063}_{-0.044}$
2.25–2.50	$1.780 \pm 0.013^{+0.053}_{-0.058}$	$1.779 \pm 0.018^{+0.060}_{-0.051}$
2.50–2.75	$1.920 \pm 0.013^{+0.056}_{-0.058}$	$1.928 \pm 0.019^{+0.069}_{-0.056}$
2.75–3.00	$2.027 \pm 0.013^{+0.061}_{-0.060}$	$2.135 \pm 0.019^{+0.082}_{-0.061}$
3.00–3.25	$1.995 \pm 0.013^{+0.060}_{-0.066}$	$2.152 \pm 0.019^{+0.077}_{-0.063}$
3.25–3.50	$1.816 \pm 0.012^{+0.054}_{-0.055}$	$2.121 \pm 0.018^{+0.073}_{-0.063}$
3.50–3.75	$1.575 \pm 0.011^{+0.047}_{-0.068}$	$1.953 \pm 0.017^{+0.078}_{-0.058}$
3.75–4.00	$1.241 \pm 0.009^{+0.040}_{-0.037}$	$1.705 \pm 0.016^{+0.054}_{-0.052}$
4.00–4.25	$0.901 \pm 0.008^{+0.028}_{-0.037}$	$1.412 \pm 0.014^{+0.046}_{-0.042}$
4.25–4.50	$0.603 \pm 0.006^{+0.020}_{-0.022}$	$1.038 \pm 0.012^{+0.038}_{-0.033}$
4.50–4.75	$0.376 \pm 0.005^{+0.012}_{-0.028}$	$0.731 \pm 0.010^{+0.027}_{-0.033}$
4.75–5.00	$0.232 \pm 0.004^{+0.007}_{-0.012}$	$0.463 \pm 0.007^{+0.019}_{-0.026}$
5.00–5.25	$0.133 \pm 0.003^{+0.004}_{-0.009}$	$0.288 \pm 0.006^{+0.009}_{-0.018}$
5.25–5.50	$0.070 \pm 0.002^{+0.002}_{-0.004}$	$0.163 \pm 0.005^{+0.005}_{-0.009}$
5.50–5.75	$0.047 \pm 0.002^{+0.002}_{-0.002}$	$0.097 \pm 0.004^{+0.006}_{-0.006}$
5.75–6.00	$0.023 \pm 0.002^{+0.002}_{-0.003}$	$0.049 \pm 0.003^{+0.002}_{-0.006}$
6.00–6.25	$0.013 \pm 0.002^{+0.003}_{-0.002}$	$0.026 \pm 0.003^{+0.004}_{-0.007}$
6.25–6.50	$0.007 \pm 0.003^{+0.006}_{-0.016}$	$0.017 \pm 0.004^{+0.005}_{-0.006}$
6.50–6.75	$0.024 \pm 0.022^{+0.006}_{-0.001}$	$0.011 \pm 0.006^{+0.010}_{-0.013}$

Table 3. The bin-averaged scaled momentum spectra, $1/N\ dn^{\pm}/d\ln(1/x_p)$, for $640 < Q^2 < 2560\,\mathrm{GeV}^2$. The first uncertainty is statistical, the second systematic.

6 Results

6.1 Scaled momentum spectra

Scaled momentum spectra were measured in the current region in the Breit frame as a function of Q^2 in the kinematic range $160 < Q^2 < 40960\,\mathrm{GeV}^2$ and $0.002 < x < 0.75$.

JHEP06(2010)009

$\ln(1/x_p)$	$2560 < Q^2 < 5120\,\mathrm{GeV}^2$	$5120 < Q^2 < 10240\,\mathrm{GeV}^2$
0.00–0.25	$0.0246 \pm 0.0028^{+0.0036}_{-0.0011}$	$0.0261 \pm 0.0044^{+0.0033}_{-0.0019}$
0.25–0.50	$0.105 \pm 0.008^{+0.005}_{-0.003}$	$0.075 \pm 0.010^{+0.008}_{-0.003}$
0.50–0.75	$0.210 \pm 0.012^{+0.014}_{-0.006}$	$0.178 \pm 0.017^{+0.018}_{-0.004}$
0.75–1.00	$0.362 \pm 0.016^{+0.031}_{-0.011}$	$0.362 \pm 0.026^{+0.044}_{-0.010}$
1.00–1.25	$0.58 \pm 0.02^{+0.03}_{-0.02}$	$0.630 \pm 0.035^{+0.055}_{-0.018}$
1.25–1.50	$0.78 \pm 0.02^{+0.03}_{-0.02}$	$0.700 \pm 0.037^{+0.069}_{-0.019}$
1.50–1.75	$1.06 \pm 0.03^{+0.07}_{-0.03}$	$1.02 \pm 0.04^{+0.11}_{-0.03}$
1.75–2.00	$1.32 \pm 0.03^{+0.08}_{-0.04}$	$1.28 \pm 0.05^{+0.09}_{-0.03}$
2.00–2.25	$1.49 \pm 0.03^{+0.10}_{-0.04}$	$1.54 \pm 0.05^{+0.14}_{-0.04}$
2.25–2.50	$1.73 \pm 0.03^{+0.08}_{-0.05}$	$1.87 \pm 0.06^{+0.15}_{-0.06}$
2.50–2.75	$1.95 \pm 0.03^{+0.11}_{-0.06}$	$2.01 \pm 0.05^{+0.14}_{-0.06}$
2.75–3.00	$2.20 \pm 0.04^{+0.11}_{-0.06}$	$2.16 \pm 0.05^{+0.14}_{-0.06}$
3.00–3.25	$2.22 \pm 0.03^{+0.11}_{-0.06}$	$2.35 \pm 0.05^{+0.12}_{-0.07}$
3.25–3.50	$2.25 \pm 0.03^{+0.09}_{-0.07}$	$2.40 \pm 0.05^{+0.13}_{-0.07}$
3.50–3.75	$2.27 \pm 0.03^{+0.11}_{-0.07}$	$2.53 \pm 0.05^{+0.14}_{-0.08}$
3.75–4.00	$2.13 \pm 0.03^{+0.09}_{-0.07}$	$2.48 \pm 0.05^{+0.15}_{-0.08}$
4.00–4.25	$1.90 \pm 0.03^{+0.07}_{-0.06}$	$2.39 \pm 0.05^{+0.13}_{-0.08}$
4.25–4.50	$1.51 \pm 0.02^{+0.05}_{-0.06}$	$2.06 \pm 0.04^{+0.12}_{-0.06}$
4.50–4.75	$1.17 \pm 0.02^{+0.04}_{-0.05}$	$1.78 \pm 0.04^{+0.08}_{-0.06}$
4.75–5.00	$0.828 \pm 0.017^{+0.030}_{-0.043}$	$1.45 \pm 0.04^{+0.10}_{-0.08}$
5.00–5.25	$0.547 \pm 0.014^{+0.019}_{-0.035}$	$0.97 \pm 0.03^{+0.06}_{-0.07}$
5.25–5.50	$0.345 \pm 0.011^{+0.012}_{-0.040}$	$0.67 \pm 0.02^{+0.05}_{-0.05}$
5.50–5.75	$0.188 \pm 0.009^{+0.008}_{-0.020}$	$0.388 \pm 0.018^{+0.041}_{-0.051}$
5.75–6.00	$0.126 \pm 0.008^{+0.005}_{-0.023}$	$0.269 \pm 0.017^{+0.022}_{-0.027}$
6.00–6.25	$0.077 \pm 0.008^{+0.004}_{-0.005}$	$0.126 \pm 0.015^{+0.024}_{-0.022}$
6.25–6.50	$0.033 \pm 0.007^{+0.004}_{-0.009}$	$0.112 \pm 0.018^{+0.022}_{-0.013}$
6.50–6.75	$0.027 \pm 0.010^{+0.001}_{-0.017}$	$0.058 \pm 0.019^{+0.016}_{-0.011}$

Table 4. The bin-averaged scaled momentum spectra, $1/N\ dn^{\pm}/d\ln(1/x_p)$, for $2560 < Q^2 < 10240\,\mathrm{GeV}^2$. The first uncertainty is statistical, the second systematic.

Results are presented in figures 1–4 and tables 2–9. Also shown in figures 1–4 are previously published results for $10 < Q^2 < 160\,\mathrm{GeV}^2$. In addition, in figure 1 data from a previous ZEUS publication [3] are given for $160 < Q^2 < 320\,\mathrm{GeV}^2$. They agree well with the measurements presented here. The same is true for previously obtained results up to

JHEP06(2010)009

$\ln(1/x_p)$	$10240 < Q^2 < 20480\,\mathrm{GeV}^2$
0.0–0.5	$0.062 \pm 0.011^{+0.007}_{-0.001}$
0.5–1.0	$0.220 \pm 0.028^{+0.039}_{-0.006}$
1.0–1.5	$0.570 \pm 0.047^{+0.087}_{-0.017}$
1.5–2.0	$1.12 \pm 0.07^{+0.15}_{-0.04}$
2.0–2.5	$1.37 \pm 0.07^{+0.19}_{-0.04}$
2.5–3.0	$2.12 \pm 0.08^{+0.20}_{-0.06}$
3.0–3.5	$2.60 \pm 0.08^{+0.18}_{-0.10}$
3.5–4.0	$2.56 \pm 0.07^{+0.19}_{-0.08}$
4.0–4.5	$2.60 \pm 0.07^{+0.18}_{-0.09}$
4.5–5.0	$2.16 \pm 0.06^{+0.14}_{-0.08}$
5.0–5.5	$1.36 \pm 0.05^{+0.07}_{-0.06}$
5.5–6.0	$0.66 \pm 0.03^{+0.04}_{-0.04}$
6.0–6.5	$0.25 \pm 0.03^{+0.03}_{-0.02}$
6.5–7.0	$0.04 \pm 0.02^{+0.04}_{-0.02}$

Table 5. The bin-averaged scaled momentum spectra, $1/N\ dn^{\pm}/d\ln(1/x_p)$, for $10240 < Q^2 < 20480\,\mathrm{GeV}^2$. The first uncertainty is statistical, the second systematic.

$\ln(1/x_p)$	$20480 < Q^2 < 40960\,\mathrm{GeV}^2$
0.0–1.0	$0.13 \pm 0.04^{+0.03}_{-0.03}$
1.0–2.0	$0.85 \pm 0.10^{+0.10}_{-0.03}$
2.0–3.0	$1.51 \pm 0.12^{+0.22}_{-0.05}$
3.0–4.0	$2.31 \pm 0.13^{+0.27}_{-0.08}$
4.0–5.0	$2.43 \pm 0.11^{+0.24}_{-0.11}$
5.0–6.0	$1.32 \pm 0.07^{+0.17}_{-0.10}$
6.0–7.0	$0.33 \pm 0.05^{+0.07}_{-0.05}$

Table 6. The bin-averaged scaled momentum spectra, $1/N\ dn^{\pm}/d\ln(1/x_p)$, for $20480 < Q^2 < 40960\,\mathrm{GeV}^2$. The first uncertainty is statistical, the second systematic.

$Q^2 = 5120\,\mathrm{Ge\,V}^2$ which are not shown.

The normalised spectrum, $1/N\ dn^{\pm}/d\ln(1/x_p)$, with N being the number of events and $n^{\pm}$ being the number of charged particles, is shown in figures 1–2. These scaled momentum spectra exhibit a hump-backed form with an approximately Gaussian shape around the peak. The mean charged multiplicities are given by the integrals of the spectra. As Q^2 increases, the multiplicity increases and, in addition, the peak of the spectrum moves to larger values of $\ln(1/x_p)$.

JHEP06(2010)009

$\langle Q^2 \rangle$, GeV^2	$0 < x_p < 0.02$
218	$9.32 \pm 0.03^{+0.29}_{-0.75}$
440	$19.10 \pm 0.09^{+0.59}_{-0.86}$
871	$35.53 \pm 0.18^{+1.08}_{-1.47}$
1767	$61.3 \pm 0.3^{+2.1}_{-2.0}$
3530	$93.6 \pm 0.7^{+3.2}_{-3.7}$
6870	$140.1 \pm 1.3^{+8.1}_{-5.9}$
13380	$191 \pm 3^{+11}_{-6}$
25700	$218 \pm 7^{+23}_{-11}$
$\langle Q^2 \rangle$, GeV^2	$0.02 < x_p < 0.05$
218	$25.86 \pm 0.04^{+0.80}_{-0.94}$
440	$39.34 \pm 0.11^{+1.23}_{-1.18}$
871	$52.15 \pm 0.18^{+1.55}_{-1.63}$
1767	$61.6 \pm 0.3^{+2.1}_{-1.8}$
3530	$68.3 \pm 0.5^{+2.9}_{-2.0}$
6870	$74.6 \pm 0.8^{+4.0}_{-2.3}$
13380	$78.6 \pm 1.7^{+5.6}_{-2.7}$
25700	$69 \pm 4^{+8}_{-2}$
$\langle Q^2 \rangle$, GeV^2	$0.05 < x_p < 0.1$
218	$19.79 \pm 0.03^{+0.63}_{-0.61}$
440	$25.34 \pm 0.07^{+0.78}_{-0.74}$
871	$26.67 \pm 0.11^{+0.78}_{-0.79}$
1767	$27.20 \pm 0.16^{+0.98}_{-0.79}$
3530	$27.6 \pm 0.3^{+1.3}_{-0.8}$
6870	$28.0 \pm 0.5^{+2.0}_{-0.8}$
13380	$26.8 \pm 0.9^{+2.9}_{-0.7}$
25700	$23.3 \pm 2.1^{+2.8}_{-0.8}$

Table 7. The number of charged particles per event and unit of x_p, $1/N\ n^{\pm}/\Delta x_p$, as a function of Q^2 in bins of x_p with widths Δx_p. The first uncertainty is statistical, the second systematic.

In figure 1, the predictions of ARIADNE and LEPTO are compared to the data. They reproduce the main features of the data but do not agree in detail. For the highest Q^2 bin, both models predict too many charged particles at medium and low values of $\ln(1/x_p)$. LEPTO also predicts too many particles for medium-Q^2 bins while ARIADNE predicts too few for low-Q^2 bins.

JHEP06(2010)009

$\langle Q^2 \rangle$, GeV^2	$0.1 < x_p < 0.2$
218	$9.338 \pm 0.015^{+0.30}_{-0.29}$
440	$10.39 \pm 0.03^{+0.32}_{-0.30}$
871	$9.92 \pm 0.05^{+0.30}_{-0.32}$
1767	$9.68 \pm 0.07^{+0.38}_{-0.28}$
3530	$9.51 \pm 0.13^{+0.63}_{-0.28}$
6870	$9.6 \pm 0.2^{+0.8}_{-0.3}$
13380	$8.5 \pm 0.4^{+1.2}_{-0.3}$
25700	$7.9 \pm 0.9^{+1.3}_{-0.3}$
$\langle Q^2 \rangle$, GeV^2	$0.2 < x_p < 0.3$
218	$4.03 \pm 0.01^{+0.13}_{-0.12}$
440	$3.89 \pm 0.02^{+0.14}_{-0.11}$
871	$3.60 \pm 0.03^{+0.11}_{-0.12}$
1767	$3.52 \pm 0.04^{+0.13}_{-0.10}$
3530	$3.29 \pm 0.08^{+0.19}_{-0.10}$
6870	$3.06 \pm 0.12^{+0.33}_{-0.09}$
13380	$2.87 \pm 0.24^{+0.37}_{-0.08}$
25700	$3.1 \pm 0.6^{+0.5}_{-0.3}$
$\langle Q^2 \rangle$, GeV^2	$0.3 < x_p < 0.4$
218	$1.806 \pm 0.007^{+0.057}_{-0.053}$
440	$1.717 \pm 0.013^{+0.070}_{-0.050}$
871	$1.515 \pm 0.019^{+0.047}_{-0.046}$
1767	$1.49 \pm 0.03^{+0.08}_{-0.04}$
3530	$1.51 \pm 0.05^{+0.09}_{-0.05}$
6870	$1.65 \pm 0.09^{+0.14}_{-0.04}$
13380	$1.33 \pm 0.16^{+0.18}_{-0.12}$
25700	$0.7 \pm 0.3^{+0.6}_{-0.4}$

Table 8. The number of charged particles per event and unit of x_p, $1/N\ n^{\pm}/\Delta x_p$, as a function of Q^2 in bins of x_p with widths Δx_p. The first uncertainty is statistical, the second systematic.

In figure 2, the MLLA+LPHD predictions [10, 18] are compared to the data. Too many particles are predicted for the highest- and lowest-Q^2 bins, while at medium Q^2 the data is reasonably well described. At low Q^2, the observed particle deficit can be interpreted as a significant migration of particles to the target region of the Breit frame; this was also previously observed [1, 2]. At medium Q^2, the agreement is surprising, because BGF contributes significantly to the cross section and the observed particles should reflect the $q\bar{q}$ final state

JHEP06(2010)009

$\langle Q^2 \rangle$, GeV^2	$0.4 < x_p < 0.5$
218	$0.868 \pm 0.005^{+0.028}_{-0.027}$
440	$0.785 \pm 0.009^{+0.031}_{-0.023}$
871	$0.716 \pm 0.013^{+0.022}_{-0.025}$
1767	$0.721 \pm 0.019^{+0.040}_{-0.021}$
3530	$0.692 \pm 0.036^{+0.053}_{-0.021}$
6870	$0.714 \pm 0.057^{+0.081}_{-0.018}$
13380	$0.392 \pm 0.086^{+0.089}_{-0.013}$
25700	$0.68 \pm 0.34^{+0.19}_{-0.16}$
$\langle Q^2 \rangle$, GeV^2	$0.5 < x_p < 0.7$
218	$0.329 \pm 0.002^{+0.010}_{-0.010}$
440	$0.295 \pm 0.004^{+0.009}_{-0.008}$
871	$0.269 \pm 0.006^{+0.009}_{-0.010}$
1767	$0.249 \pm 0.008^{+0.015}_{-0.007}$
3530	$0.277 \pm 0.015^{+0.016}_{-0.008}$
6870	$0.197 \pm 0.020^{+0.024}_{-0.006}$
13380	$0.257 \pm 0.045^{+0.054}_{-0.006}$
25700	$0.33 \pm 0.15^{+0.11}_{-0.07}$
$\langle Q^2 \rangle$, GeV^2	$0.7 < x_p < 1.0$
218	$0.056 \pm 0.001^{+0.002}_{-0.002}$
440	$0.046 \pm 0.001^{+0.001}_{-0.001}$
871	$0.041 \pm 0.002^{+0.001}_{-0.002}$
1767	$0.042 \pm 0.002^{+0.001}_{-0.003}$
3530	$0.049 \pm 0.004^{+0.004}_{-0.001}$
6870	$0.043 \pm 0.006^{+0.003}_{-0.002}$
13380	$0.054 \pm 0.012^{+0.007}_{-0.002}$
25700	$0.013 \pm 0.013^{+0.002}_{-0.021}$

Table 9. The number of charged particles per event and unit of x_p, $1/N\ n^{\pm}/\Delta x_p$, as a function of Q^2 in bins of x_p with widths Δx_p. The first uncertainty is statistical, the second systematic.

which is not included in the prediction. At the highest Q^2 available, the failure of the MLLA prediction probably reflects the fact that the e^+e^- data used to obtain the input parameters are dominated by Z^0 exchange while, in ep collisions, photon exchange still dominates.

The MLLA+LPHD calculations predict long tails towards large values of $\ln(1/x_p)$ over the complete range of Q^2. These tails are sensitive to the mass correction applied in the calculation [19, 67]. The data do not show such tails in the predicted size. A better

JHEP06(2010)009

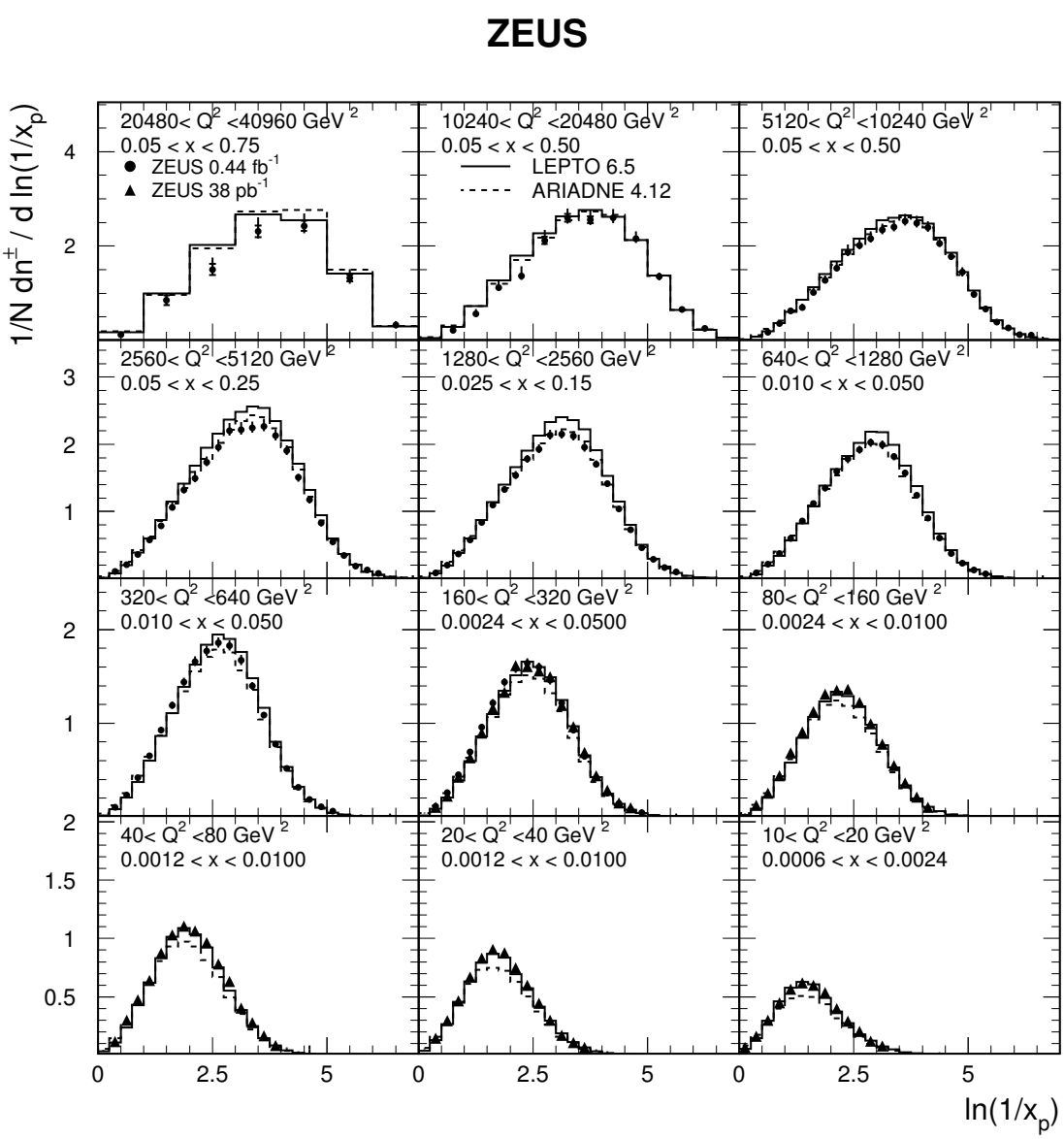

Figure 1. The scaled momentum spectra, $1/N\ dn^{\pm}/d\ln(1/x_p)$, for different (x, Q^2) bins. The dots represent the new, the triangles the previous ZEUS measurement. The data overlap in the $160 < Q^2 < 320\,GeV^2$ bin. The inner error bars, where visible, indicate statistical uncertainties, the outer statistical and systematic uncertainties added in quadrature. The full and dashed lines represent the LEPTO and the ARIADNE predictions, respectively.

description of the large $\ln(1/x_p)$ region is obtained if $m_{\rm eff} = Q_0 = 0.9\Lambda_{\rm eff}$ is taken instead of $m_{\rm eff} = Q_0 = \Lambda_{\rm eff}$.

6.2 Scaling violation

As the energy scale, Q, increases, the phase space for soft gluon radiation increases, leading to a rise of the number of soft particles with small x_p. These scaling violations can be seen when the data are plotted in bins of x_p as a function of Q^2. Figure 3 and

JHEP06(2010)009

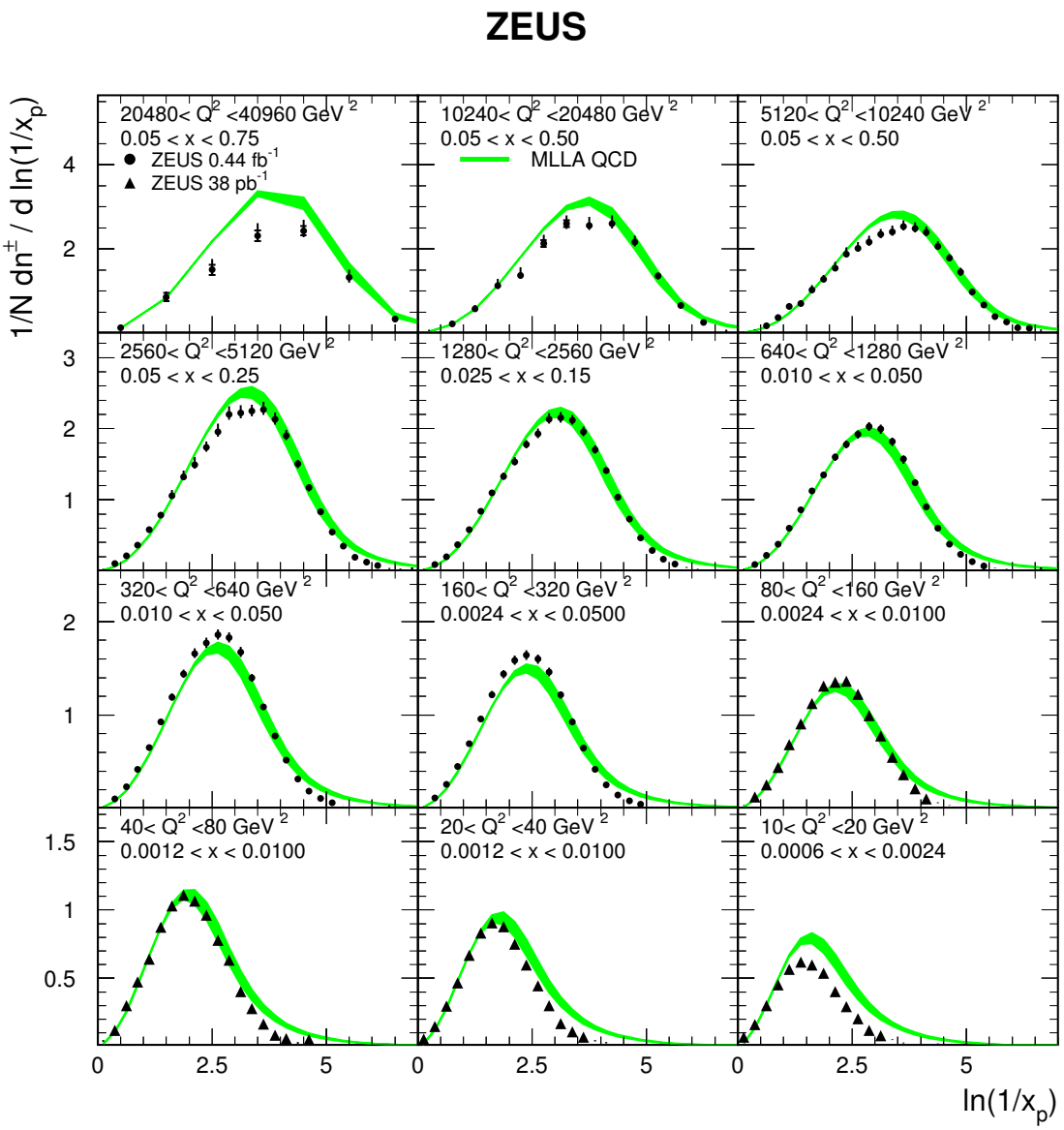

Figure 2. The scaled momentum spectra, $1/N\ dn^{\pm}/d\ln(1/x_p)$, for different (x, Q^2) bins. The band represents the range of the MLLA+LPHD predictions. Other details as in figure 1.

tables 7–9 show that the number of charged particles increases with Q^2 at low x_p and decreases with Q^2 at high x_p. Neither LEPTO nor ARIADNE provides a good description of this Q^2 dependence over the whole range of x_p.

Figure 4 shows the data together with four NLO+FF QCD predictions [12–17] for $x_p > 0.1$, where theoretical uncertainties are small and the predictions not too strongly affected by hadron-mass effects which are not included in the calculations [52]. The fragmentation functions (FF) used in all four calculations were extracted from e^+e^- data. The four predictions are similar in shape and have similar uncertainties. The uncertainties are only illustrated for the calculation of Kretzer [12]. The NLO calculations also do not

JHEP06(2010)009

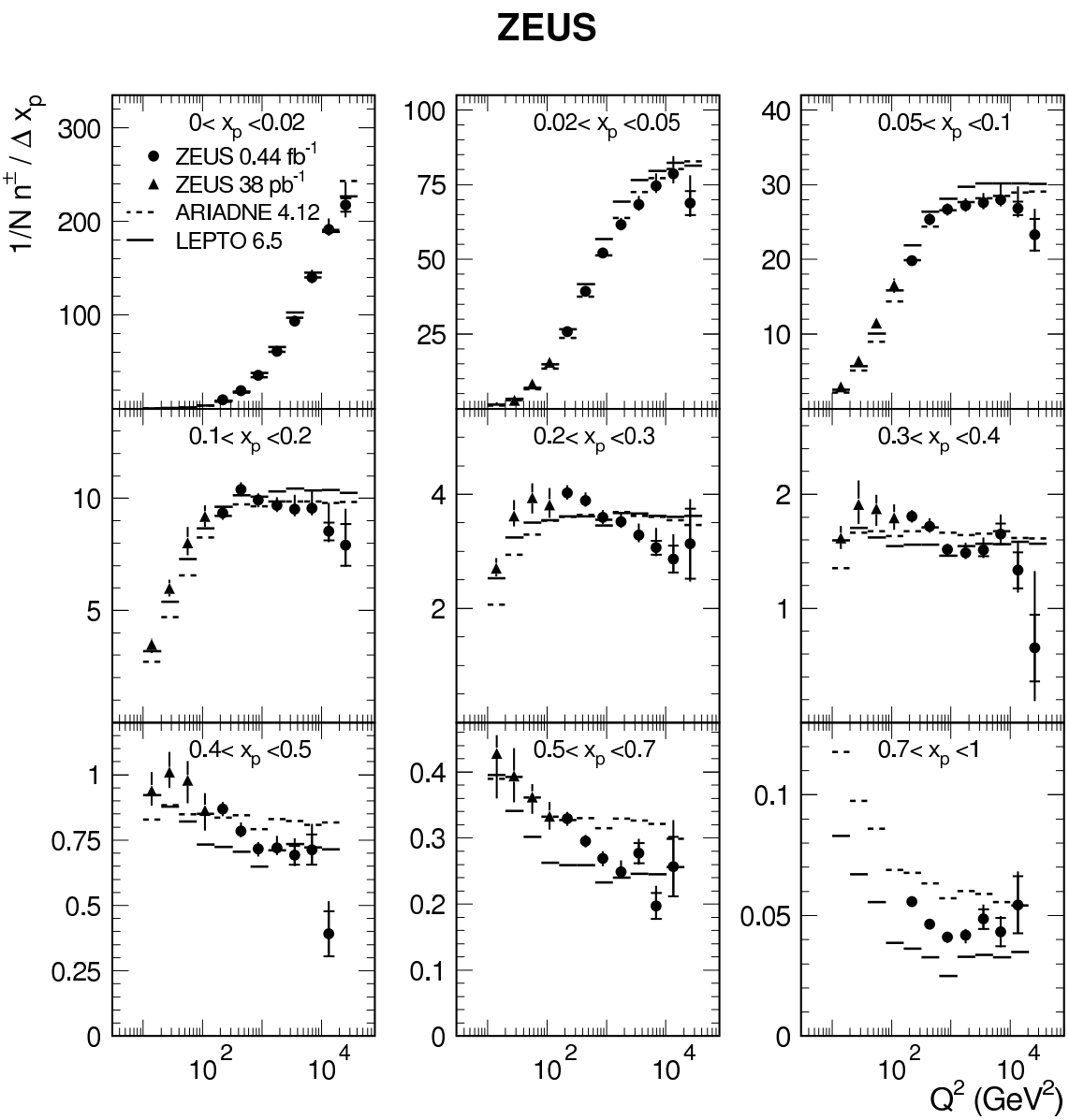

Figure 3. The number of charged particles per event per unit of x_p, $1/N\ n^{\pm}/\Delta x_p$, as a function of Q^2 in x_p bins of width Δx_p. Other details as in figure 1.

provide a good description of the data. Too many particles are predicted at small x_p and too few at large x_p. In general, the scaling violations predicted are not strong enough.

Figure 5 shows the same data as figure 4 together with results from H1 [4] and from e^+e^- experiments [20–23]. For a proper comparison, the the particle momenta from e^+e^- data were scaled to half of the centre-of-mass energy as discussed in the introduction and the scale was set to $Q = 2\ E_{\rm beam}$, where $E_{\rm beam}$ is the beam energy. In addition, corrections for the different treatment of K^0 and Λ decays were applied. The overall agreement between the different data sets supports fragmentation universality. The presentation of the data using a linear scale as presented in figure 6 does, however, show some significant differences

JHEP06(2010)009

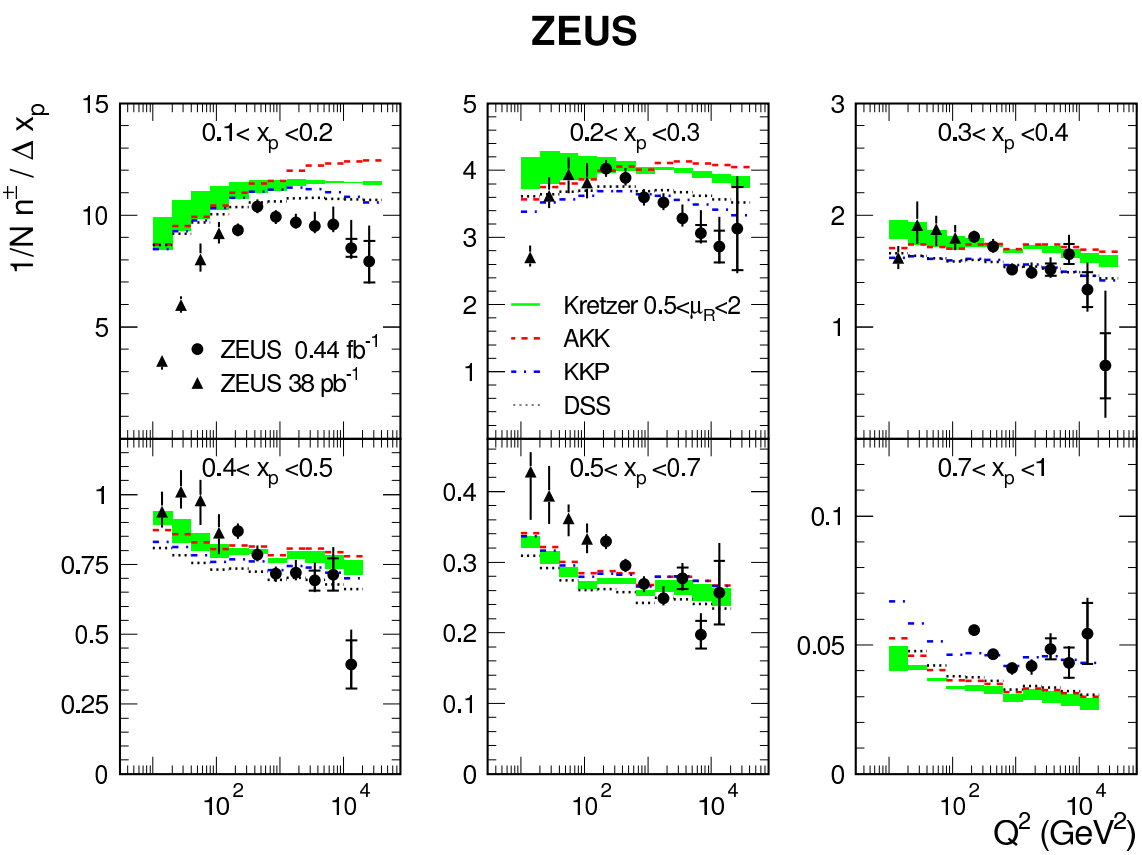

Figure 4. The number of charged particles per event per unit of x_p, $1/N\ n^{\pm}/\Delta x_p$, as a function of Q^2 in x_p bins with width Δx_p as in figure 3. The shaded band represents the NLO calculation by Kretzer [12] with its renormalisation scale uncertainty. Additional NLO calculations are shown: Kniehl, Kramer, Pötter [13](KKP), Albino, Kniehl, Kramer [14](AKK) and De Florian, Sassot and Stratmann [16, 17](DSS).

between e^+e^- and ep, in particular around the Z^0 mass at $0.02 < x_p < 0.2$ and at low Q^2 at $0.1 < x_p < 0.2$.

6.3 Limiting fragmentation

The concept of limiting fragmentation [25] is based on the assumption that a Lorentz-contracted object passes through another object at rest, leaving behind an excited state with properties depending neither on the energy nor the identity of the passing object. This excited state fragments into particles in a restricted window of rapidity, called the limiting-fragmentation region. In this region, the limiting-fragmentation hypothesis predicts that the density of charged particles per unit of rapidity depends only on W.

Limiting fragmentation has been observed in a variety of hadronic collisions [68–70], including nucleus-nucleus interactions [26–30]. It was observed that in the region of limiting fragmentation the particle density increases linearly with the rapidity before reaching a plateau. The slope of the increase did not show a W dependence, but the height of the plateau increased with W. These features are illustrated in figure 7. Bialas and Jezabek [71] proposed a statistical model to explain the missing W dependence of

JHEP06(2010)009

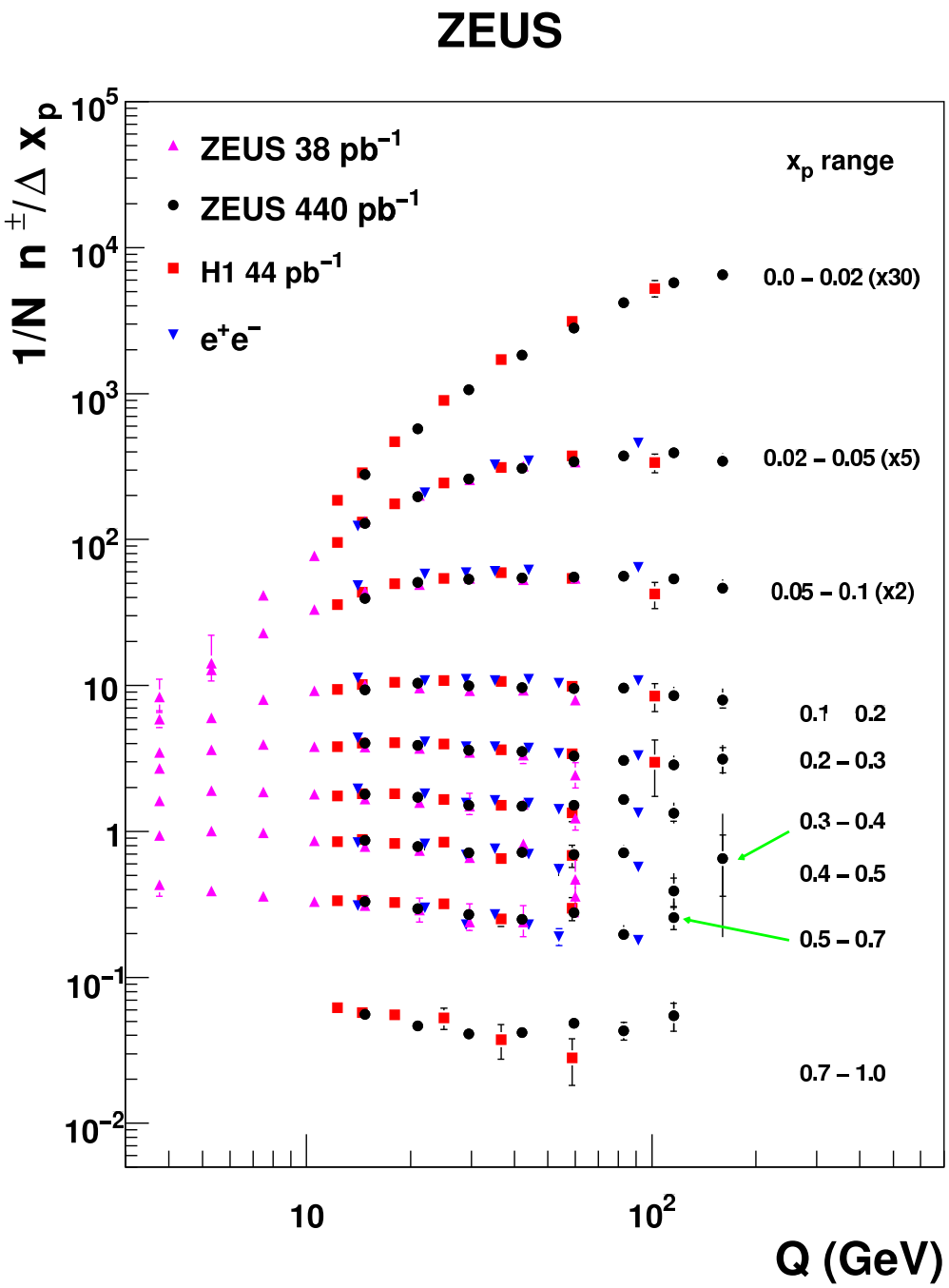

Figure 5. The number of charged particles per event per unit of x_p, $1/N\ n^{\pm}/\Delta x_p$, as a function of Q in x_p bins with width Δx_p. Also shown are data from H1 [4] and e^+e^- [20–23]. The dots (triangles) represent the new (previous) ZEUS measurement, the squares the H1 data and the inverted triangles the e^+e^- data. The inner error bars, where visible, indicate statistical uncertainties, the outer statistical and systematic uncertainties added in quadrature. The three lowest x_p bins are scaled by factors of 30, 5 and 2, respectively.

JHEP06(2010)009

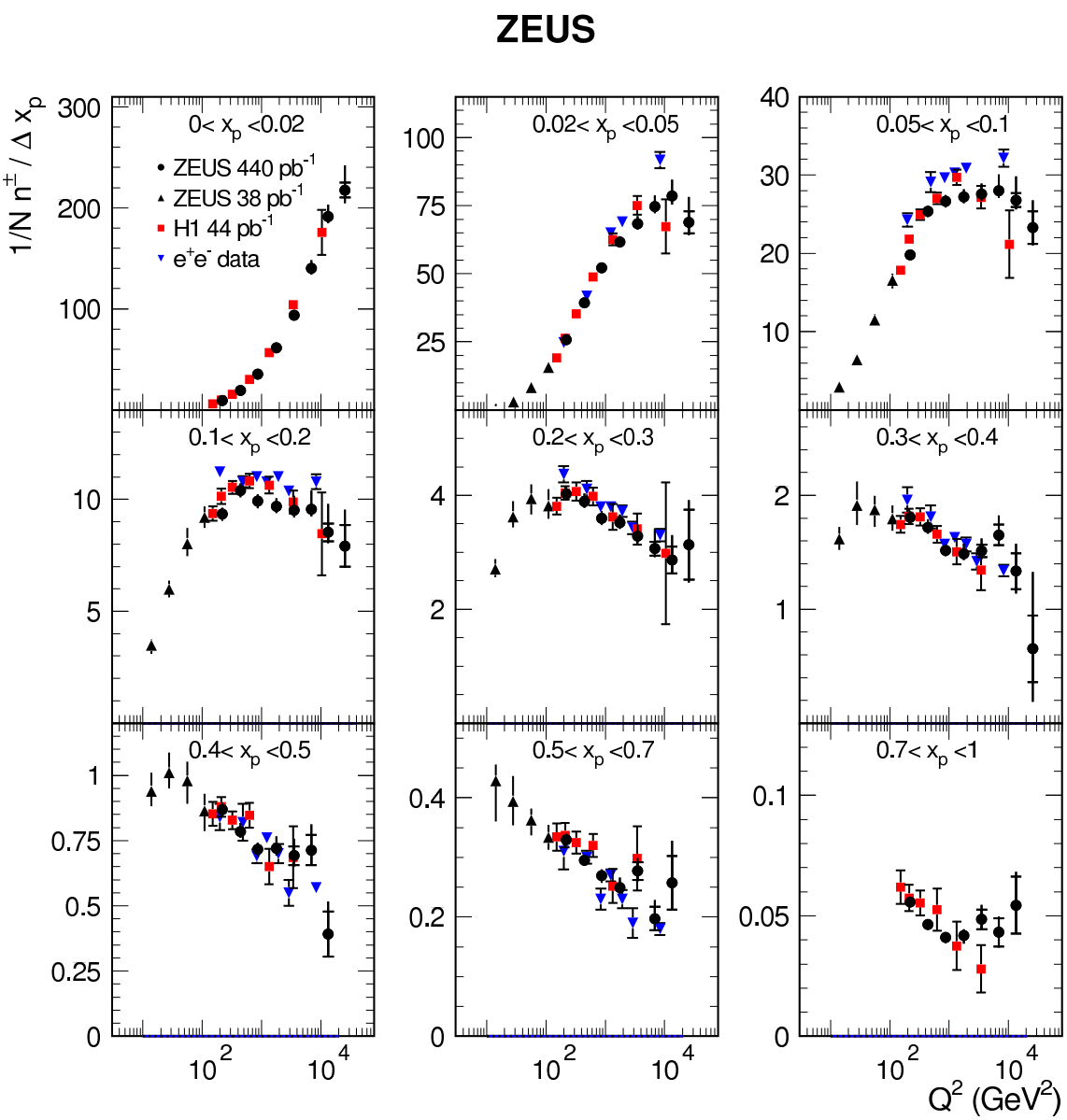

Figure 6. The number of charged particles per event per unit of x_p, $1/N\ n^{\pm}/\Delta x_p$, as a function of Q^2 in x_p bins with width Δx_p. Other details as in figure 5.

the slopes. In this model, soft particle production in hadronic collisions is described in terms of multiple gluon exchanges between partons of the colliding hadrons and by the subsequent radiation of hadronic clusters.

The application of the limiting-fragmentation hypothesis to e^+e^- annihilations is not straight-forward. However, again a behaviour as illustrated in figure 7 was observed, only in this case the slopes increase with W [70, 72].

In the case of ep collisions, the passing object is the proton while the virtual photon exchanged in the interaction is the object "at rest". It is assumed to be the excited hadron which fragments [72].

JHEP06(2010)009

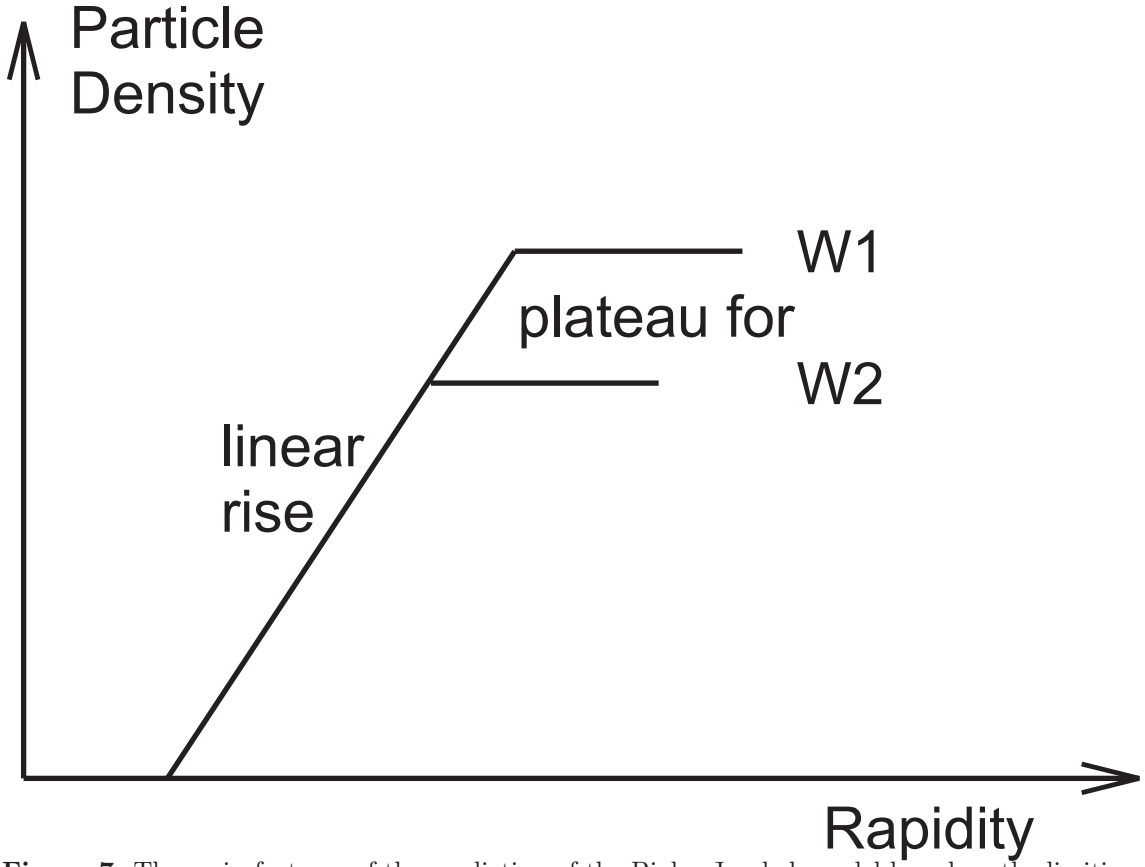

Figure 7. The main features of the prediction of the Bialas-Jezabek model based on the limiting-fragmentation hypothesis for the dependence of the particles density on the rapidity in hadronic collisions for two values of W with $W1 > W2$.

Figures 8–9 and tables 10–15 present the density of charged particles per unit of pseudorapidity, η^{Breit}, for $10 < Q^2 < 10240$ GeV^2 in bins of Q^2 and W as listed in table 1. A region of linear rise and the onset of a plateau are observed in all bins. This supports the applicability of the hypothesis of limiting fragmentation to the case of ep collisions. However, for low Q^2, the plateau is only reached in the target region, $\eta^{\text{Breit}} > 0$.

The slopes in the region of linear rise do not depend significantly on either Q^2 or W, as also demonstrated in figures 10 and 11. The lack of a W dependence indicates that the model of Bialas and Jezabek is also applicable for ep collisions.

Figures 8 and 9 also show predictions from Ariadne and Lepto. Overall, Ariadne provides reasonable predictions for the whole range in Q^2 and W. Lepto, however, predicts a sizeable increase in the height of the plateau with Q^2 and W which is not observed in the data. The predictions in the plateau region are sensitive to the input parameters used in the fragmentation functions. The usage of input parameters derived from SMC data [73] in Lepto results in the prediction of a softer spectrum, reflected in a charged-particle density of up to 30 % too high.

The hypothesis of limiting fragmentation was further tested by studying the charged-particle densities in the rest frame of the fragmenting object, i.e. the virtual photon. The

JHEP06(2010)009

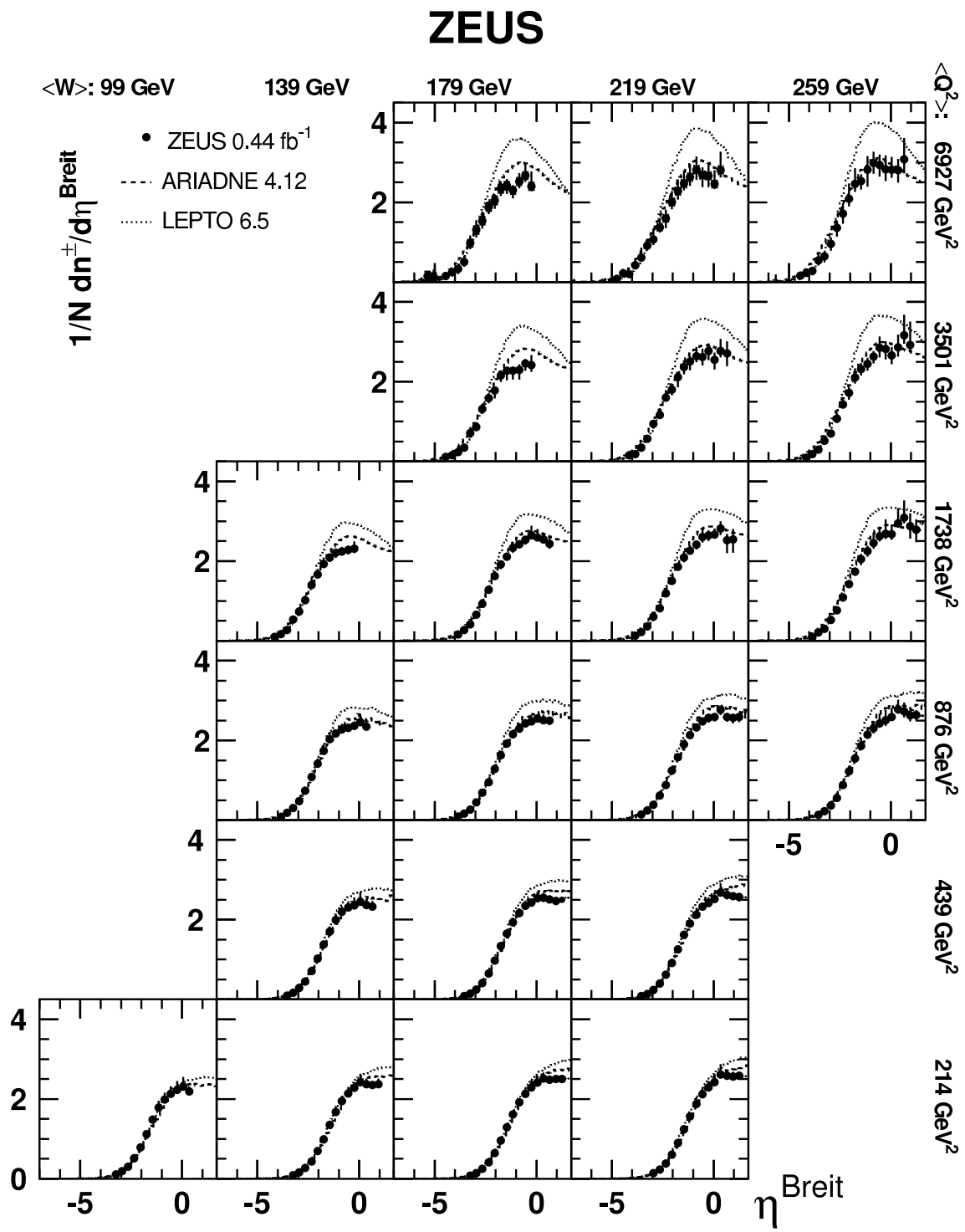

Figure 8. The normalised charged-particle density per unit of η^{Breit}, $1/N\ dn^{\pm}/d\eta^{\mathrm{Breit}}$, for different (W, Q^2) bins for $Q^2 > 160\,\mathrm{GeV}^2$. The dots represent the ZEUS measurement. The error bars, where visible, indicate statistical and systematic uncertainties added in quadrature. The dashed and dotted lines represent the LEPTO and ARIADNE predictions, respectively.

JHEP06(2010)009

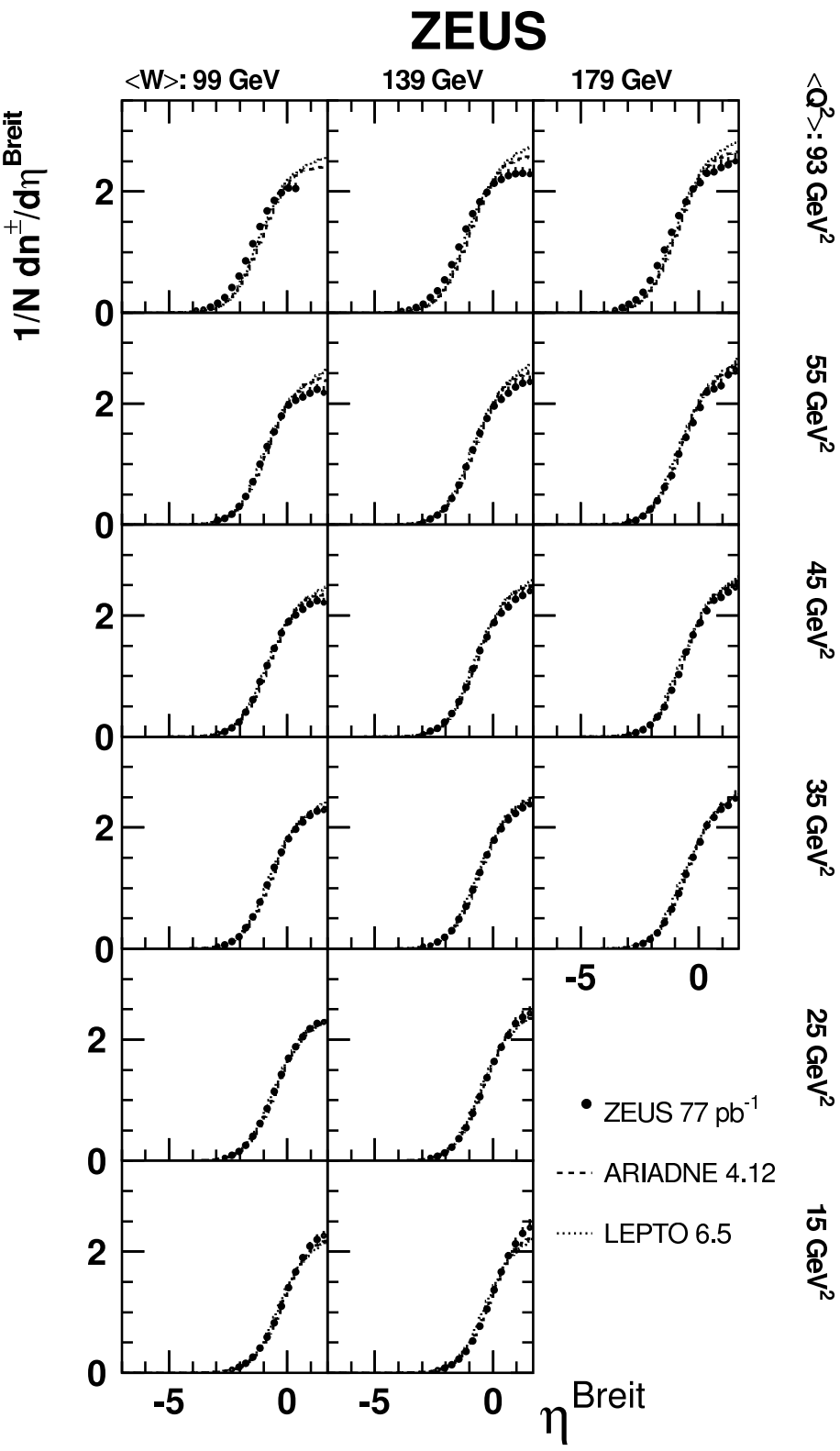

Figure 9. The normalised charged-particle density per unit of η^{Breit}, $1/N\ dn^{\pm}/d\eta^{\mathrm{Breit}}$, for different (W, Q^2) bins for $10 < Q^2 < 160\,\mathrm{GeV}^2$. Other details as in figure 8.

JHEP06(2010)009

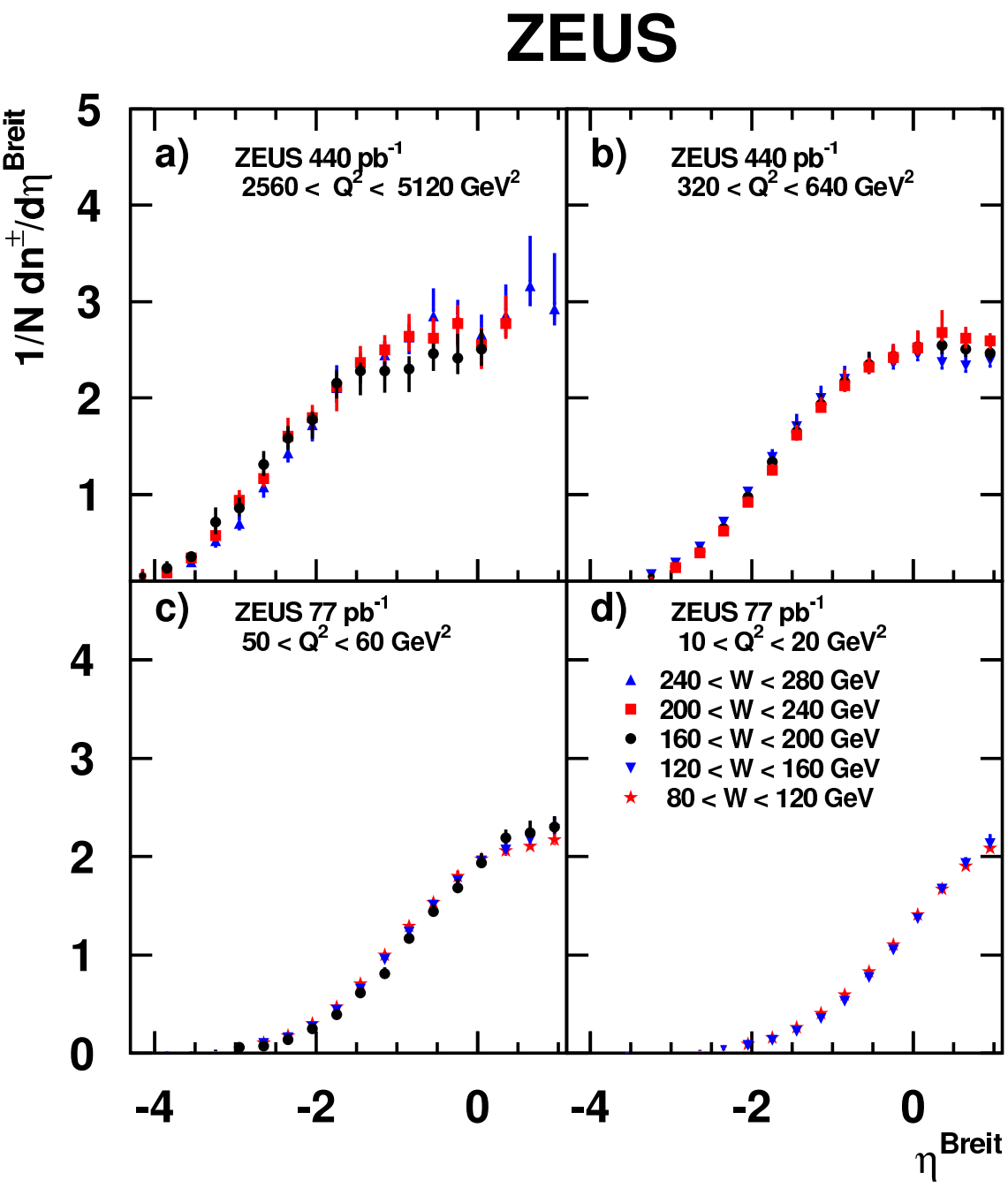

Figure 10. The normalised charged-particle density per unit of η^{Breit}, $1/N\ dn^{\pm}/d\eta^{\mathrm{Breit}}$, for 4 bins in Q^2 and 5 bins in W. The error bars, where visible, indicate statistical and systematic uncertainties added in quadrature.

η^{Breit} distributions were rebinned by shifting event by event all entries by $\ln(Q/m_\pi)$, thus scaling the available energy to the pion mass. The resulting distributions are shown in figure 11. The distributions are very similar but for $Q^2 > 160\,\mathrm{GeV}^2$ a slightly larger slope is observed. This is a region where the BGF contribution is decreasing. In general, the

JHEP06(2010)009

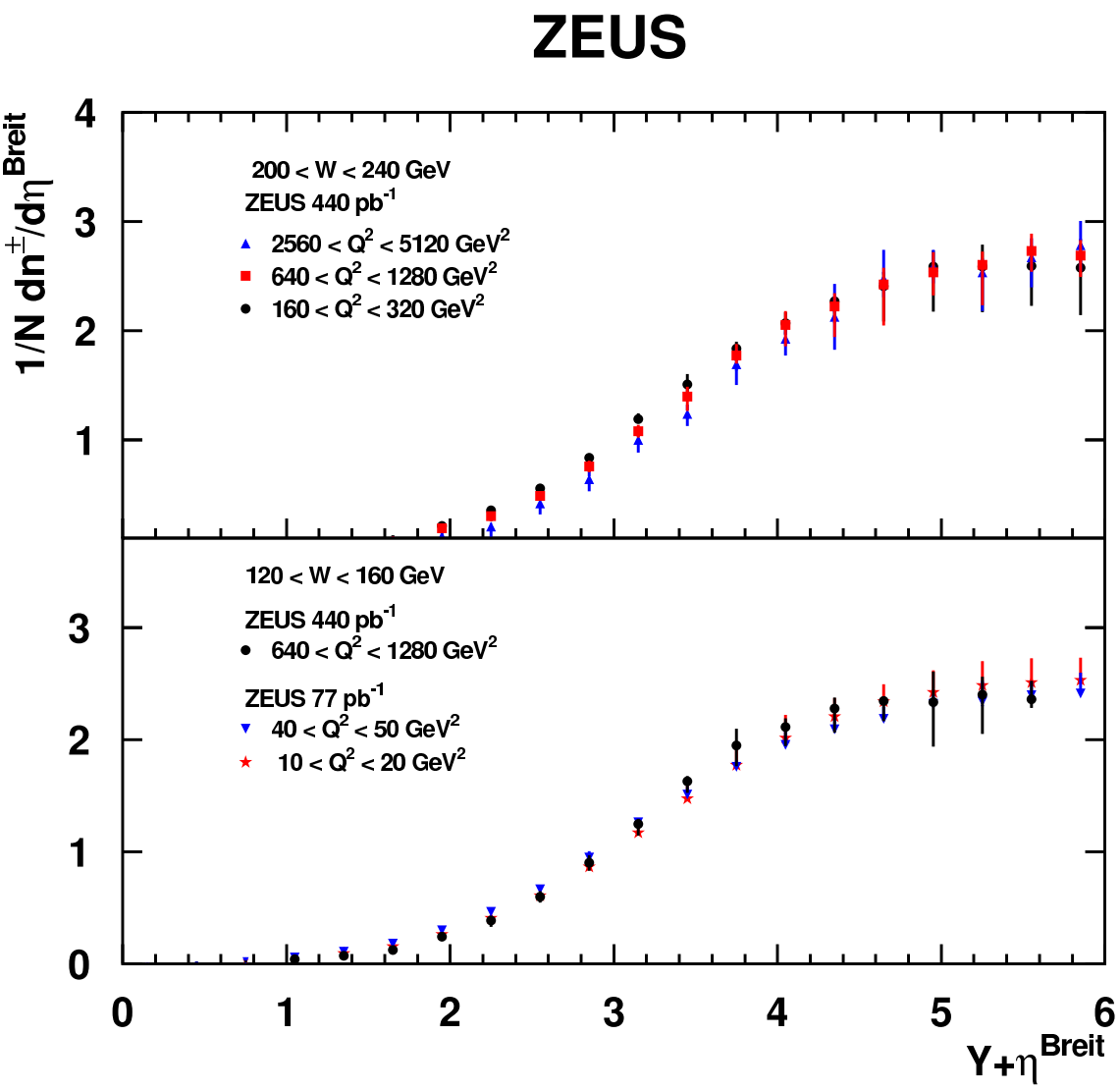

Figure 11. The normalised charged-particle density per unit of $\eta^{\rm Breit}$, $1/N\ dn^{\pm}/d\eta^{\rm Breit}$, for 2 bins in W and 5 bins in Q^2. The distributions were rebinned by shifting the entries for each event by $\mathrm{Y}{=}\ln(Q/m_\pi)$ as explained in the text. The error bars, where visible, indicate statistical and systematic uncertainties added in quadrature.

observations support the hypothesis of limiting fragmentation and the model of Bialas and Jezabek. This indicates that, even at high Q^2, soft processes are involved in the fragmentation and a statistical approach is justified.

7 Conclusions

Scaled momentum spectra have been measured in NC DIS for the current region in the Breit frame over the large range of Q^2 from 10 GeV^2 to 40960 GeV^2. Large scaling violations are observed. Comparing the data to e^+e^- results generally supports the concept of quark-

η^{Breit}			$160 < W < 200\,\mathrm{GeV}$	$200 < W < 240\,\mathrm{GeV}$	$240 < W < 280\,\mathrm{GeV}$
-5.5	–	-5.2	$0.15 \pm 0.11\ ^{+0.06}_{-0.06}$	$0.054 \pm 0.027\ ^{+0.030}_{-0.006}$	$0.017 \pm 0.012\ ^{+0.015}_{-0.014}$
-5.2	–	-4.9	$0.14 \pm 0.08\ ^{+0.14}_{-0.05}$	$0.04 \pm 0.02\ ^{+0.04}_{-0.03}$	$0.027 \pm 0.016\ ^{+0.017}_{-0.053}$
-4.9	–	-4.6	$0.07 \pm 0.03\ ^{+0.04}_{-0.06}$	$0.08 \pm 0.03\ ^{+0.04}_{-0.02}$	$0.068 \pm 0.024\ ^{+0.045}_{-0.018}$
-4.6	–	-4.3	$0.15 \pm 0.04\ ^{+0.05}_{-0.04}$	$0.22 \pm 0.04\ ^{+0.11}_{-0.07}$	$0.16 \pm 0.03\ ^{+0.09}_{-0.08}$
-4.3	–	-4.0	$0.25 \pm 0.05\ ^{+0.07}_{-0.09}$	$0.20 \pm 0.04\ ^{+0.07}_{-0.04}$	$0.23 \pm 0.04\ ^{+0.06}_{-0.08}$
-4.0	–	-3.7	$0.33 \pm 0.06\ ^{+0.01}_{-0.12}$	$0.42 \pm 0.06\ ^{+0.17}_{-0.04}$	$0.28 \pm 0.04\ ^{+0.09}_{-0.10}$
-3.7	–	-3.4	$0.51 \pm 0.07\ ^{+0.14}_{-0.11}$	$0.61 \pm 0.06\ ^{+0.24}_{-0.08}$	$0.54 \pm 0.05\ ^{+0.14}_{-0.11}$
-3.4	–	-3.1	$0.97 \pm 0.09\ ^{+0.17}_{-0.12}$	$0.92 \pm 0.08\ ^{+0.15}_{-0.10}$	$0.64 \pm 0.06\ ^{+0.10}_{-0.14}$
-3.1	–	-2.8	$1.31 \pm 0.10\ ^{+0.22}_{-0.16}$	$1.07 \pm 0.08\ ^{+0.27}_{-0.12}$	$0.96 \pm 0.07\ ^{+0.15}_{-0.15}$
-2.8	–	-2.5	$1.54 \pm 0.10\ ^{+0.21}_{-0.17}$	$1.37 \pm 0.08\ ^{+0.22}_{-0.10}$	$1.36 \pm 0.08\ ^{+0.16}_{-0.20}$
-2.5	–	-2.2	$1.88 \pm 0.10\ ^{+0.09}_{-0.15}$	$1.60 \pm 0.09\ ^{+0.20}_{-0.23}$	$1.72 \pm 0.09\ ^{+0.24}_{-0.24}$
-2.2	–	-1.9	$2.05 \pm 0.10\ ^{+0.11}_{-0.19}$	$2.01 \pm 0.09\ ^{+0.25}_{-0.16}$	$2.09 \pm 0.09\ ^{+0.37}_{-0.17}$
-1.9	–	-1.6	$2.34 \pm 0.10\ ^{+0.16}_{-0.14}$	$2.28 \pm 0.09\ ^{+0.27}_{-0.19}$	$2.46 \pm 0.10\ ^{+0.38}_{-0.17}$
-1.6	–	-1.3	$2.42 \pm 0.10\ ^{+0.13}_{-0.19}$	$2.47 \pm 0.09\ ^{+0.32}_{-0.14}$	$2.54 \pm 0.10\ ^{+0.13}_{-0.19}$
-1.3	–	1.0	$2.30 \pm 0.09\ ^{+0.10}_{-0.18}$	$2.63 \pm 0.09\ ^{+0.32}_{-0.20}$	$2.81 \pm 0.10\ ^{+0.33}_{-0.41}$
-1.0	–	-0.7	$2.52 \pm 0.09\ ^{+0.20}_{-0.14}$	$2.82 \pm 0.09\ ^{+0.32}_{-0.24}$	$2.98 \pm 0.11\ ^{+0.27}_{-0.25}$
-0.7	–	-0.4	$2.67 \pm 0.09\ ^{+0.29}_{-0.12}$	$2.68 \pm 0.09\ ^{+0.18}_{-0.29}$	$2.94 \pm 0.11\ ^{+0.23}_{-0.28}$
-0.4	–	-0.1	$2.41 \pm 0.09\ ^{+0.36}_{-0.09}$	$2.66 \pm 0.09\ ^{+0.29}_{-0.27}$	$2.82 \pm 0.10\ ^{+0.34}_{-0.28}$
-0.1	–	0.2		$2.46 \pm 0.08\ ^{+0.34}_{-0.09}$	$2.81 \pm 0.10\ ^{+0.32}_{-0.18}$
0.2	–	0.5		$2.81 \pm 0.10\ ^{+0.46}_{-0.15}$	$2.80 \pm 0.10\ ^{+0.26}_{-0.29}$
0.5	–	0.8			$3.08 \pm 0.11\ ^{+0.53}_{-0.33}$

Table 10. The charged-particle density, $1/N\ dn^{\pm}/d\eta^{\mathrm{Breit}}$, for $5120 < Q^2 < 10240\,\mathrm{GeV}^{\,2}$ and 3 bins in W. The first uncertainty is statistical, the second systematic.

fragmentation universality. Neither MLLA+LPHD nor NLO+FF calculations describe the data well. A better, albeit not prefect description is provided by the ARIADNE program.

The limiting-fragmentation hypothesis and the statistical model of Bialas and Jezabek were tested by studying the density of charged particles as a function of the pseudorapidity, η^{Breit}, over the range of $10 < Q^2 < 10240\,\mathrm{GeV}^2$. A region of linear rise and the onset of a plateau are observed over the whole range in Q^2 and support the limiting fragmentation hypothesis. The independence of the slopes on W supports the statistical approach of Bialas and Jezabek.

Acknowledgments

We appreciate the contributions to the construction and maintenance of the ZEUS detector of many people who are not listed as authors. The HERA machine group and the DESY computing staff are especially acknowledged for their success in providing excellent operation of the collider and the data analysis environment. We thank the DESY directorate for their strong support and encouragement. We thank W. Khoze, W. Ochs, R. Sassot, A. Białas and M. Jeżabek for fruitful discussions. We especially would like to thank S. Albino for providing the QCD calculations and for instructive discussions.

JHEP06(2010)009

η^{Breit}	$160 < W < 200\,\text{GeV}$	$200 < W < 240\,\text{GeV}$	$240 < W < 280\,\text{GeV}$
-4.6 – -4.3	$0.112 \pm 0.019\ ^{+0.042}_{-0.012}$	$0.074 \pm 0.015\ ^{+0.019}_{-0.028}$	$0.069 \pm 0.014\ ^{+0.050}_{-0.031}$
-4.3 – -4.0	$0.16 \pm 0.02\ ^{+0.04}_{-0.03}$	$0.15 \pm 0.02\ ^{+0.07}_{-0.01}$	$0.095 \pm 0.015\ ^{+0.041}_{-0.024}$
-4.0 – -3.7	$0.24 \pm 0.03\ ^{+0.07}_{-0.02}$	$0.19 \pm 0.02\ ^{+0.08}_{-0.03}$	$0.19 \pm 0.02\ ^{+0.05}_{-0.03}$
-3.7 – -3.4	$0.35 \pm 0.03\ ^{+0.05}_{-0.04}$	$0.34 \pm 0.03\ ^{+0.05}_{-0.02}$	$0.30 \pm 0.03\ ^{+0.08}_{-0.03}$
-3.4 – -3.1	$0.71 \pm 0.04\ ^{+0.14}_{-0.12}$	$0.57 \pm 0.04\ ^{+0.08}_{-0.05}$	$0.52 \pm 0.03\ ^{+0.07}_{-0.07}$
-3.1 – -2.8	$0.86 \pm 0.04\ ^{+0.11}_{-0.07}$	$0.94 \pm 0.04\ ^{+0.10}_{-0.11}$	$0.70 \pm 0.04\ ^{+0.08}_{-0.06}$
-2.8 – -2.5	$1.31 \pm 0.05\ ^{+0.13}_{-0.11}$	$1.16 \pm 0.05\ ^{+0.16}_{-0.07}$	$1.08 \pm 0.05\ ^{+0.13}_{-0.10}$
-2.5 – -2.2	$1.59 \pm 0.05\ ^{+0.11}_{-0.12}$	$1.60 \pm 0.05\ ^{+0.18}_{-0.07}$	$1.43 \pm 0.05\ ^{+0.14}_{-0.09}$
-2.2 – -1.9	$1.78 \pm 0.05\ ^{+0.06}_{-0.20}$	$1.80 \pm 0.06\ ^{+0.12}_{-0.13}$	$1.72 \pm 0.05\ ^{+0.13}_{-0.17}$
-1.9 – -1.6	$2.15 \pm 0.06\ ^{+0.12}_{-0.15}$	$2.11 \pm 0.06\ ^{+0.11}_{-0.24}$	$2.11 \pm 0.06\ ^{+0.22}_{-0.15}$
-1.6 – -1.3	$2.28 \pm 0.06\ ^{+0.07}_{-0.24}$	$2.37 \pm 0.06\ ^{+0.16}_{-0.18}$	$2.32 \pm 0.06\ ^{+0.13}_{-0.16}$
-1.3 – -1.0	$2.28 \pm 0.05\ ^{+0.09}_{-0.22}$	$2.50 \pm 0.06\ ^{+0.13}_{-0.21}$	$2.45 \pm 0.06\ ^{+0.13}_{-0.17}$
-1.0 – -0.7	$2.30 \pm 0.05\ ^{+0.13}_{-0.24}$	$2.64 \pm 0.06\ ^{+0.23}_{-0.14}$	$2.63 \pm 0.06\ ^{+0.12}_{-0.17}$
-0.7 – -0.4	$2.46 \pm 0.05\ ^{+0.10}_{-0.17}$	$2.62 \pm 0.06\ ^{+0.21}_{-0.20}$	$2.85 \pm 0.07\ ^{+0.27}_{-0.23}$
-0.4 – -0.1	$2.41 \pm 0.05\ ^{+0.25}_{-0.16}$	$2.77 \pm 0.06\ ^{+0.19}_{-0.23}$	$2.82 \pm 0.06\ ^{+0.19}_{-0.26}$
-0.1 – 0.2		$2.55 \pm 0.06\ ^{+0.17}_{-0.24}$	$2.66 \pm 0.06\ ^{+0.20}_{-0.21}$
0.2 – 0.5		$2.77 \pm 0.06\ ^{+0.29}_{-0.15}$	$2.86 \pm 0.06\ ^{+0.31}_{-0.23}$
0.5 – 0.8		$2.71 \pm 0.07\ ^{+0.30}_{-0.31}$	$3.16 \pm 0.07\ ^{+0.52}_{-0.20}$
0.8 – 1.1			$2.92 \pm 0.07\ ^{+0.58}_{-0.15}$

Table 11. The charged-particle density, $1/N\ dn^{\pm}/d\eta^{\text{Breit}}$, for $2560 < Q^2 < 5120\,\text{GeV}^2$ and 3 bins in W. The first uncertainty is statistical, the second systematic.

η^{Breit}	$120 < W < 160\,\text{GeV}$	$160 < W < 200\,\text{GeV}$	$200 < W < 240\,\text{GeV}$	$240 < W < 280\,\text{GeV}$
-4.3 – -4.0	$0.103 \pm 0.010\ ^{+0.052}_{-0.014}$	$0.071 \pm 0.008\ ^{+0.013}_{-0.016}$	$0.071 \pm 0.008\ ^{+0.013}_{-0.018}$	$0.057 \pm 0.007\ ^{+0.022}_{-0.011}$
-4.0 – -3.7	$0.170 \pm 0.013\ ^{+0.010}_{-0.036}$	$0.161 \pm 0.012\ ^{+0.022}_{-0.025}$	$0.127 \pm 0.010\ ^{+0.025}_{-0.027}$	$0.088 \pm 0.008\ ^{+0.025}_{-0.010}$
-3.7 – -3.4	$0.268 \pm 0.016\ ^{+0.043}_{-0.034}$	$0.264 \pm 0.015\ ^{+0.046}_{-0.034}$	$0.218 \pm 0.013\ ^{+0.030}_{-0.036}$	$0.203 \pm 0.012\ ^{+0.028}_{-0.011}$
-3.4 – -3.1	$0.53 \pm 0.02\ ^{+0.10}_{-0.05}$	$0.414 \pm 0.018\ ^{+0.070}_{-0.032}$	$0.359 \pm 0.017\ ^{+0.032}_{-0.035}$	$0.300 \pm 0.014\ ^{+0.053}_{-0.035}$
-3.1 – -2.8	$0.73 \pm 0.02\ ^{+0.07}_{-0.03}$	$0.65 \pm 0.02\ ^{+0.07}_{-0.04}$	$0.61 \pm 0.02\ ^{+0.10}_{-0.04}$	$0.524 \pm 0.019\ ^{+0.055}_{-0.029}$
-2.8 – -2.5	$1.02 \pm 0.03\ ^{+0.12}_{-0.06}$	$0.93 \pm 0.03\ ^{+0.08}_{-0.05}$	$0.81 \pm 0.02\ ^{+0.06}_{-0.08}$	$0.77 \pm 0.02\ ^{+0.03}_{-0.07}$
-2.5 – -2.2	$1.41 \pm 0.03\ ^{+0.20}_{-0.09}$	$1.28 \pm 0.03\ ^{+0.05}_{-0.07}$	$1.19 \pm 0.03\ ^{+0.10}_{-0.06}$	$1.09 \pm 0.03\ ^{+0.07}_{-0.09}$
-2.2 – -1.9	$1.67 \pm 0.03\ ^{+0.13}_{-0.09}$	$1.62 \pm 0.03\ ^{+0.12}_{-0.06}$	$1.50 \pm 0.03\ ^{+0.09}_{-0.09}$	$1.42 \pm 0.03\ ^{+0.08}_{-0.08}$
-1.9 – -1.6	$1.93 \pm 0.03\ ^{+0.15}_{-0.09}$	$1.92 \pm 0.03\ ^{+0.08}_{-0.12}$	$1.85 \pm 0.03\ ^{+0.10}_{-0.08}$	$1.74 \pm 0.03\ ^{+0.09}_{-0.10}$
-1.6 – -1.3	$2.09 \pm 0.03\ ^{+0.10}_{-0.11}$	$2.11 \pm 0.03\ ^{+0.09}_{-0.08}$	$2.08 \pm 0.03\ ^{+0.16}_{-0.11}$	$2.04 \pm 0.03\ ^{+0.13}_{-0.15}$
-1.3 – -1.0	$2.21 \pm 0.03\ ^{+0.09}_{-0.13}$	$2.33 \pm 0.03\ ^{+0.14}_{-0.11}$	$2.26 \pm 0.04\ ^{+0.12}_{-0.07}$	$2.25 \pm 0.04\ ^{+0.13}_{-0.13}$
-1.0 – -0.7	$2.24 \pm 0.03\ ^{+0.11}_{-0.09}$	$2.42 \pm 0.03\ ^{+0.10}_{-0.09}$	$2.41 \pm 0.04\ ^{+0.10}_{-0.12}$	$2.45 \pm 0.04\ ^{+0.24}_{-0.14}$
-0.7 – -0.4	$2.28 \pm 0.03\ ^{+0.10}_{-0.10}$	$2.53 \pm 0.03\ ^{+0.09}_{-0.11}$	$2.60 \pm 0.04\ ^{+0.19}_{-0.13}$	$2.62 \pm 0.04\ ^{+0.23}_{-0.13}$
-0.4 – -0.1	$2.31 \pm 0.03\ ^{+0.18}_{-0.11}$	$2.65 \pm 0.03\ ^{+0.24}_{-0.09}$	$2.64 \pm 0.04\ ^{+0.13}_{-0.14}$	$2.68 \pm 0.04\ ^{+0.36}_{-0.12}$
-0.1 – 0.2		$2.60 \pm 0.03\ ^{+0.21}_{-0.09}$	$2.66 \pm 0.04\ ^{+0.15}_{-0.09}$	$2.68 \pm 0.04\ ^{+0.23}_{-0.14}$
0.2 – 0.5		$2.54 \pm 0.03\ ^{+0.16}_{-0.10}$	$2.81 \pm 0.04\ ^{+0.18}_{-0.16}$	$2.95 \pm 0.04\ ^{+0.38}_{-0.11}$
0.5 – 0.8		$2.43 \pm 0.04\ ^{+0.18}_{-0.12}$	$2.52 \pm 0.04\ ^{+0.16}_{-0.32}$	$3.08 \pm 0.04\ ^{+0.44}_{-0.13}$
0.8 – 1.1			$2.54 \pm 0.04\ ^{+0.25}_{-0.33}$	$2.88 \pm 0.04\ ^{+0.32}_{-0.32}$
1.1 – 1.3				$2.79 \pm 0.04\ ^{+0.26}_{-0.32}$

Table 12. The charged-particle density, $1/N\ dn^{\pm}/d\eta^{\text{Breit}}$, for $1280 < Q^2 < 2560\,\text{GeV}^2$ and 4 bins in W. The first uncertainty is statistical, the second systematic.

JHEP06(2010)009

η^{Breit}	$120 < W < 160\,\text{GeV}$	$160 < W < 200\,\text{GeV}$	$200 < W < 240\,\text{GeV}$	$240 < W < 280\,\text{GeV}$
-4.0 – -3.7	$0.086 \pm 0.006\ ^{+0.014}_{-0.016}$	$0.087 \pm 0.006\ ^{+0.008}_{-0.014}$	$0.073 \pm 0.005\ ^{+0.014}_{-0.008}$	$0.069 \pm 0.005\ ^{+0.022}_{-0.006}$
-3.7 – -3.4	$0.185 \pm 0.008\ ^{+0.032}_{-0.018}$	$0.159 \pm 0.007\ ^{+0.020}_{-0.007}$	$0.138 \pm 0.007\ ^{+0.011}_{-0.017}$	$0.130 \pm 0.007\ ^{+0.021}_{-0.031}$
-3.4 – -3.1	$0.301 \pm 0.010\ ^{+0.036}_{-0.019}$	$0.263 \pm 0.009\ ^{+0.038}_{-0.033}$	$0.238 \pm 0.009\ ^{+0.040}_{-0.008}$	$0.224 \pm 0.009\ ^{+0.020}_{-0.015}$
-3.1 – -2.8	$0.476 \pm 0.013\ ^{+0.036}_{-0.034}$	$0.444 \pm 0.012\ ^{+0.059}_{-0.018}$	$0.387 \pm 0.011\ ^{+0.027}_{-0.026}$	$0.364 \pm 0.012\ ^{+0.049}_{-0.016}$
-2.8 – -2.5	$0.735 \pm 0.015\ ^{+0.040}_{-0.062}$	$0.683 \pm 0.015\ ^{+0.096}_{-0.029}$	$0.617 \pm 0.014\ ^{+0.035}_{-0.027}$	$0.559 \pm 0.014\ ^{+0.038}_{-0.039}$
-2.5 – -2.2	$1.080 \pm 0.018\ ^{+0.086}_{-0.052}$	$0.950 \pm 0.017\ ^{+0.085}_{-0.048}$	$0.881 \pm 0.017\ ^{+0.056}_{-0.048}$	$0.874 \pm 0.018\ ^{+0.097}_{-0.035}$
-2.2 – -1.9	$1.418 \pm 0.019\ ^{+0.128}_{-0.058}$	$1.283 \pm 0.019\ ^{+0.048}_{-0.041}$	$1.25 \pm 0.02\ ^{+0.10}_{-0.05}$	$1.22 \pm 0.02\ ^{+0.14}_{-0.04}$
-1.9 – -1.6	$1.74 \pm 0.02\ ^{+0.16}_{-0.06}$	$1.62 \pm 0.02\ ^{+0.10}_{-0.07}$	$1.58 \pm 0.02\ ^{+0.19}_{-0.06}$	$1.54 \pm 0.02\ ^{+0.12}_{-0.05}$
-1.6 – -1.3	$2.03 \pm 0.02\ ^{+0.18}_{-0.09}$	$1.92 \pm 0.02\ ^{+0.11}_{-0.06}$	$1.90 \pm 0.02\ ^{+0.16}_{-0.11}$	$1.86 \pm 0.02\ ^{+0.18}_{-0.06}$
-1.3 – -1.0	$2.17 \pm 0.02\ ^{+0.08}_{-0.07}$	$2.15 \pm 0.02\ ^{+0.11}_{-0.08}$	$2.13 \pm 0.02\ ^{+0.19}_{-0.07}$	$2.15 \pm 0.03\ ^{+0.19}_{-0.06}$
-1.0 – -0.7	$2.27 \pm 0.02\ ^{+0.14}_{-0.09}$	$2.29 \pm 0.02\ ^{+0.08}_{-0.10}$	$2.33 \pm 0.03\ ^{+0.17}_{-0.08}$	$2.31 \pm 0.03\ ^{+0.15}_{-0.13}$
-0.7 – -0.4	$2.31 \pm 0.02\ ^{+0.11}_{-0.08}$	$2.43 \pm 0.02\ ^{+0.11}_{-0.08}$	$2.48 \pm 0.03\ ^{+0.17}_{-0.08}$	$2.43 \pm 0.03\ ^{+0.24}_{-0.11}$
-0.4 – -0.1	$2.37 \pm 0.02\ ^{+0.11}_{-0.09}$	$2.48 \pm 0.02\ ^{+0.14}_{-0.07}$	$2.56 \pm 0.03\ ^{+0.24}_{-0.12}$	$2.50 \pm 0.03\ ^{+0.25}_{-0.14}$
-0.1 – 0.2	$2.45 \pm 0.02\ ^{+0.21}_{-0.07}$	$2.55 \pm 0.02\ ^{+0.11}_{-0.07}$	$2.59 \pm 0.03\ ^{+0.21}_{-0.11}$	$2.59 \pm 0.03\ ^{+0.22}_{-0.10}$
0.2 – 0.5	$2.35 \pm 0.02\ ^{+0.18}_{-0.08}$	$2.51 \pm 0.02\ ^{+0.14}_{-0.10}$	$2.77 \pm 0.03\ ^{+0.25}_{-0.13}$	$2.78 \pm 0.03\ ^{+0.25}_{-0.10}$
0.5 – 0.8		$2.49 \pm 0.02\ ^{+0.10}_{-0.11}$	$2.58 \pm 0.02\ ^{+0.14}_{-0.11}$	$2.73 \pm 0.03\ ^{+0.22}_{-0.15}$
0.8 – 1.1			$2.57 \pm 0.03\ ^{+0.11}_{-0.14}$	$2.63 \pm 0.03\ ^{+0.21}_{-0.16}$
1.1 – 1.4			$2.59 \pm 0.03\ ^{+0.15}_{-0.13}$	$2.64 \pm 0.03\ ^{+0.11}_{-0.14}$

Table 13. The charged-particle density, $1/N\ dn^{\pm}/d\eta^{\text{Breit}}$, for $640 < Q^2 < 1280\,\text{GeV}^2$ and 4 bins in W. The first uncertainty is statistical, the second systematic.

η^{Breit}	$120 < W < 160\,\text{GeV}$	$160 < W < 200\,\text{GeV}$	$200 < W < 240\,\text{GeV}$
-3.7 – -3.4	$0.094 \pm 0.003\ ^{+0.013}_{-0.011}$	$0.083 \pm 0.003\ ^{+0.008}_{-0.008}$	$0.082 \pm 0.004\ ^{+0.010}_{-0.013}$
-3.4 – -3.1	$0.168 \pm 0.005\ ^{+0.009}_{-0.017}$	$0.145 \pm 0.004\ ^{+0.013}_{-0.012}$	$0.134 \pm 0.004\ ^{+0.009}_{-0.012}$
-3.1 – -2.8	$0.285 \pm 0.006\ ^{+0.019}_{-0.018}$	$0.246 \pm 0.006\ ^{+0.013}_{-0.023}$	$0.241 \pm 0.006\ ^{+0.014}_{-0.013}$
-2.8 – -2.5	$0.451 \pm 0.007\ ^{+0.016}_{-0.032}$	$0.404 \pm 0.007\ ^{+0.015}_{-0.019}$	$0.395 \pm 0.007\ ^{+0.031}_{-0.028}$
-2.5 – -2.2	$0.714 \pm 0.009\ ^{+0.039}_{-0.033}$	$0.646 \pm 0.009\ ^{+0.037}_{-0.025}$	$0.621 \pm 0.009\ ^{+0.024}_{-0.029}$
-2.2 – -1.9	$1.022 \pm 0.010\ ^{+0.049}_{-0.042}$	$0.969 \pm 0.011\ ^{+0.052}_{-0.040}$	$0.915 \pm 0.011\ ^{+0.060}_{-0.033}$
-1.9 – -1.6	$1.384 \pm 0.012\ ^{+0.084}_{-0.049}$	$1.335 \pm 0.012\ ^{+0.058}_{-0.045}$	$1.253 \pm 0.013\ ^{+0.065}_{-0.051}$
-1.6 – -1.3	$1.702 \pm 0.013\ ^{+0.133}_{-0.069}$	$1.652 \pm 0.013\ ^{+0.099}_{-0.077}$	$1.618 \pm 0.014\ ^{+0.103}_{-0.057}$
-1.3 – -1.0	$1.998 \pm 0.013\ ^{+0.133}_{-0.051}$	$1.936 \pm 0.014\ ^{+0.105}_{-0.067}$	$1.903 \pm 0.015\ ^{+0.102}_{-0.052}$
-1.0 – -0.7	$2.192 \pm 0.013\ ^{+0.140}_{-0.050}$	$2.166 \pm 0.015\ ^{+0.121}_{-0.066}$	$2.129 \pm 0.016\ ^{+0.165}_{-0.064}$
-0.7 – -0.4	$2.305 \pm 0.013\ ^{+0.158}_{-0.054}$	$2.350 \pm 0.015\ ^{+0.126}_{-0.074}$	$2.323 \pm 0.017\ ^{+0.095}_{-0.068}$
-0.4 – -0.1	$2.356 \pm 0.013\ ^{+0.203}_{-0.061}$	$2.434 \pm 0.016\ ^{+0.101}_{-0.071}$	$2.422 \pm 0.018\ ^{+0.136}_{-0.069}$
-0.1 – 0.2	$2.447 \pm 0.013\ ^{+0.241}_{-0.065}$	$2.536 \pm 0.015\ ^{+0.160}_{-0.068}$	$2.522 \pm 0.017\ ^{+0.175}_{-0.073}$
0.2 – 0.5	$2.364 \pm 0.013\ ^{+0.169}_{-0.071}$	$2.549 \pm 0.015\ ^{+0.124}_{-0.095}$	$2.680 \pm 0.017\ ^{+0.230}_{-0.092}$
0.5 – 0.8	$2.332 \pm 0.014\ ^{+0.139}_{-0.069}$	$2.505 \pm 0.015\ ^{+0.093}_{-0.080}$	$2.617 \pm 0.017\ ^{+0.120}_{-0.102}$
0.8 – 1.1		$2.468 \pm 0.015\ ^{+0.097}_{-0.081}$	$2.591 \pm 0.016\ ^{+0.081}_{-0.080}$
1.1 – 1.4		$2.500 \pm 0.016\ ^{+0.101}_{-0.091}$	$2.569 \pm 0.017\ ^{+0.071}_{-0.105}$

Table 14. The charged-particle density, $1/N\ dn^{\pm}/d\eta^{\text{Breit}}$, for $320 < Q^2 < 640\,\text{GeV}^2$ and 3 bins in W. The first uncertainty is statistical, the second systematic.

JHEP06(2010)009

$\eta^{\rm Breit}$	$80 < W < 120\,\text{GeV}$	$120 < W < 160\,\text{GeV}$	$160 < W < 200\,\text{GeV}$	$200 < W = 240\,\text{GeV}$
-3.4 – -3.1	$0.107 \pm 0.002\ ^{+0.007}_{-0.007}$	$0.092 \pm 0.002\ ^{+0.004}_{-0.005}$	$0.082 \pm 0.002\ ^{+0.003}_{-0.005}$	$0.079 \pm 0.002\ ^{+0.005}_{-0.005}$
-3.1 – -2.8	$0.186 \pm 0.003\ ^{+0.006}_{-0.010}$	$0.155 \pm 0.002\ ^{+0.004}_{-0.015}$	$0.144 \pm 0.003\ ^{+0.008}_{-0.012}$	$0.136 \pm 0.003\ ^{+0.004}_{-0.012}$
-2.8 – -2.5	$0.304 \pm 0.004\ ^{+0.010}_{-0.011}$	$0.270 \pm 0.003\ ^{+0.012}_{-0.016}$	$0.248 \pm 0.003\ ^{+0.011}_{-0.015}$	$0.233 \pm 0.004\ ^{+0.012}_{-0.010}$
-2.5 – -2.2	$0.512 \pm 0.005\ ^{+0.017}_{-0.020}$	$0.436 \pm 0.004\ ^{+0.015}_{-0.018}$	$0.411 \pm 0.004\ ^{+0.011}_{-0.017}$	$0.386 \pm 0.005\ ^{+0.016}_{-0.031}$
-2.2 – -1.9	$0.790 \pm 0.006\ ^{+0.023}_{-0.030}$	$0.695 \pm 0.005\ ^{+0.018}_{-0.022}$	$0.646 \pm 0.005\ ^{+0.020}_{-0.020}$	$0.609 \pm 0.006\ ^{+0.020}_{-0.037}$
-1.9 – -1.6	$1.119 \pm 0.006\ ^{+0.045}_{-0.042}$	$0.992 \pm 0.006\ ^{+0.033}_{-0.020}$	$0.959 \pm 0.006\ ^{+0.034}_{-0.032}$	$0.902 \pm 0.007\ ^{+0.035}_{-0.038}$
-1.6 – -1.3	$1.479 \pm 0.007\ ^{+0.108}_{-0.058}$	$1.349 \pm 0.007\ ^{+0.080}_{-0.040}$	$1.288 \pm 0.007\ ^{+0.049}_{-0.034}$	$1.242 \pm 0.008\ ^{+0.072}_{-0.040}$
-1.3 – -1.0	$1.783 \pm 0.007\ ^{+0.173}_{-0.056}$	$1.679 \pm 0.007\ ^{+0.143}_{-0.041}$	$1.619 \pm 0.008\ ^{+0.078}_{-0.048}$	$1.568 \pm 0.009\ ^{+0.082}_{-0.057}$
-1.0 – -0.7	$1.989 \pm 0.007\ ^{+0.167}_{-0.054}$	$1.947 \pm 0.008\ ^{+0.132}_{-0.052}$	$1.918 \pm 0.009\ ^{+0.104}_{-0.056}$	$1.880 \pm 0.010\ ^{+0.165}_{-0.079}$
-0.7 – -0.4	$2.126 \pm 0.007\ ^{+0.197}_{-0.059}$	$2.140 \pm 0.008\ ^{+0.164}_{-0.061}$	$2.134 \pm 0.009\ ^{+0.145}_{-0.060}$	$2.120 \pm 0.011\ ^{+0.159}_{-0.073}$
-0.4 – -0.1	$2.233 \pm 0.007\ ^{+0.223}_{-0.066}$	$2.277 \pm 0.008\ ^{+0.143}_{-0.060}$	$2.294 \pm 0.010\ ^{+0.183}_{-0.065}$	$2.288 \pm 0.011\ ^{+0.165}_{-0.061}$
-0.1 – 0.2	$2.309 \pm 0.007\ ^{+0.242}_{-0.066}$	$2.421 \pm 0.008\ ^{+0.211}_{-0.067}$	$2.417 \pm 0.010\ ^{+0.173}_{-0.052}$	$2.424 \pm 0.011\ ^{+0.204}_{-0.070}$
0.2 – 0.5	$2.190 \pm 0.008\ ^{+0.127}_{-0.067}$	$2.376 \pm 0.008\ ^{+0.140}_{-0.056}$	$2.513 \pm 0.010\ ^{+0.151}_{-0.064}$	$2.617 \pm 0.011\ ^{+0.258}_{-0.072}$
0.5 – 0.8		$2.354 \pm 0.008\ ^{+0.098}_{-0.068}$	$2.485 \pm 0.009\ ^{+0.105}_{-0.069}$	$2.587 \pm 0.011\ ^{+0.151}_{-0.066}$
0.8 – 1.1		$2.377 \pm 0.009\ ^{+0.135}_{-0.070}$	$2.501 \pm 0.009\ ^{+0.075}_{-0.056}$	$2.569 \pm 0.011\ ^{+0.114}_{-0.074}$
1.1 – 1.4			$2.500 \pm 0.010\ ^{+0.070}_{-0.070}$	$2.587 \pm 0.011\ ^{+0.094}_{-0.075}$

Table 15. The charged-particle density, $1/N\ dn^{\pm}/d\eta^{\rm Breit}$, for $160 < Q^2 < 320\,\text{GeV}^{\,2}$ and 4 bins in W. The first uncertainty is statistical, the second systematic.

$\eta^{\rm Breit}$	$80 < W < 120\,\text{GeV}$	$120 < W < 160\,\text{GeV}$	$160 < W < 200\,\text{GeV}$
-4.0 – -3.7	$0.034 \pm 0.002^{+0.001}_{-0.002}$	$0.033 \pm 0.002^{+0.002}_{-0.002}$	$0.027 \pm 0.002^{+0.002}_{-0.001}$
-3.7 – -3.4	$0.057 \pm 0.002^{+0.003}_{-0.001}$	$0.053 \pm 0.003^{+0.002}_{-0.003}$	$0.049 \pm 0.003^{+0.002}_{-0.002}$
-3.4 – -3.1	$0.093 \pm 0.003^{+0.003}_{-0.001}$	$0.086 \pm 0.003^{+0.002}_{-0.001}$	$0.084 \pm 0.004^{+0.004}_{-0.004}$
-3.1 – -2.8	$0.158 \pm 0.004^{+0.005}_{-0.004}$	$0.141 \pm 0.004^{+0.007}_{-0.002}$	$0.138 \pm 0.004^{+0.004}_{-0.004}$
-2.8 – -2.5	$0.254 \pm 0.005^{+0.006}_{-0.005}$	$0.248 \pm 0.005^{+0.006}_{-0.004}$	$0.214 \pm 0.005^{+0.004}_{-0.004}$
-2.5 – -2.2	$0.413 \pm 0.006^{+0.012}_{-0.008}$	$0.361 \pm 0.006^{+0.011}_{-0.005}$	$0.339 \pm 0.006^{+0.007}_{-0.006}$
-2.2 – -1.9	$0.600 \pm 0.007^{+0.019}_{-0.010}$	$0.542 \pm 0.007^{+0.012}_{-0.008}$	$0.530 \pm 0.008^{+0.007}_{-0.011}$
-1.9 – -1.6	$0.856 \pm 0.008^{+0.023}_{-0.013}$	$0.796 \pm 0.009^{+0.012}_{-0.008}$	$0.773 \pm 0.009^{+0.009}_{-0.012}$
-1.6 – -1.3	$1.140 \pm 0.009^{+0.025}_{-0.010}$	$1.084 \pm 0.010^{+0.008}_{-0.011}$	$1.034 \pm 0.011^{+0.016}_{-0.011}$
-1.3 – -1.0	$1.424 \pm 0.010^{+0.032}_{-0.011}$	$1.383 \pm 0.011^{+0.016}_{-0.013}$	$1.324 \pm 0.012^{+0.020}_{-0.014}$
-1.0 – -0.7	$1.682 \pm 0.011^{+0.027}_{-0.015}$	$1.634 \pm 0.012^{+0.025}_{-0.009}$	$1.600 \pm 0.013^{+0.022}_{-0.015}$
-0.7 – -0.4	$1.855 \pm 0.011^{+0.032}_{-0.017}$	$1.833 \pm 0.012^{+0.031}_{-0.013}$	$1.827 \pm 0.014^{+0.045}_{-0.015}$
-0.4 – -0.1	$1.979 \pm 0.012^{+0.063}_{-0.021}$	$1.986 \pm 0.013^{+0.065}_{-0.025}$	$2.039 \pm 0.014^{+0.042}_{-0.012}$
-0.1 – 0.2	$2.060 \pm 0.012^{+0.075}_{-0.020}$	$2.134 \pm 0.013^{+0.069}_{-0.022}$	$2.142 \pm 0.014^{+0.081}_{-0.020}$
0.2 – 0.5	$2.051 \pm 0.012^{+0.093}_{-0.044}$	$2.201 \pm 0.013^{+0.093}_{-0.031}$	$2.301 \pm 0.014^{+0.092}_{-0.032}$
0.5 – 0.8	$2.082 \pm 0.012^{+0.100}_{-0.025}$	$2.263 \pm 0.013^{+0.107}_{-0.017}$	$2.327 \pm 0.014^{+0.116}_{-0.033}$
0.8 – 1.1		$2.294 \pm 0.013^{+0.111}_{-0.038}$	$2.395 \pm 0.014^{+0.139}_{-0.030}$
1.1 – 1.4		$2.302 \pm 0.013^{+0.104}_{-0.025}$	$2.440 \pm 0.015^{+0.126}_{-0.033}$
1.4 – 1.7		$2.287 \pm 0.014^{+0.092}_{-0.026}$	$2.497 \pm 0.015^{+0.139}_{-0.018}$

Table 16. The charged-particle density, $1/N\ dn^{\pm}/d\eta^{\rm Breit}$, for $60 < Q^2 < 160\,\text{GeV}^{\,2}$ and 3 bins in W. The first uncertainty is statistical, the second systematic.

JHEP06(2010)009

η^{Breit}	$80 < W < 120\,\text{GeV}$	$120 < W < 160\,\text{GeV}$	$160 < W < 200\,\text{GeV}$
-3.1 – -2.8	$0.070 \pm 0.005^{+0.010}_{-0.008}$	$0.051 \pm 0.004^{+0.008}_{-0.003}$	$0.057 \pm 0.005^{+0.009}_{-0.005}$
-2.8 – -2.5	$0.105 \pm 0.005^{+0.005}_{-0.005}$	$0.096 \pm 0.006^{+0.013}_{-0.006}$	$0.073 \pm 0.005^{+0.005}_{-0.004}$
-2.5 – -2.2	$0.177 \pm 0.007^{+0.014}_{-0.007}$	$0.157 \pm 0.007^{+0.009}_{-0.009}$	$0.139 \pm 0.008^{+0.010}_{-0.007}$
-2.2 – -1.9	$0.298 \pm 0.009^{+0.015}_{-0.012}$	$0.271 \pm 0.010^{+0.016}_{-0.010}$	$0.250 \pm 0.010^{+0.011}_{-0.014}$
-1.9 – -1.6	$0.469 \pm 0.011^{+0.016}_{-0.015}$	$0.436 \pm 0.012^{+0.012}_{-0.013}$	$0.391 \pm 0.012^{+0.024}_{-0.015}$
-1.6 – -1.3	$0.706 \pm 0.014^{+0.028}_{-0.009}$	$0.654 \pm 0.014^{+0.021}_{-0.018}$	$0.611 \pm 0.016^{+0.036}_{-0.019}$
-1.3 – -1.0	$0.999 \pm 0.016^{+0.021}_{-0.026}$	$0.951 \pm 0.017^{+0.021}_{-0.019}$	$0.809 \pm 0.017^{+0.062}_{-0.016}$
-1.0 – -0.7	$1.293 \pm 0.018^{+0.035}_{-0.020}$	$1.233 \pm 0.019^{+0.023}_{-0.027}$	$1.17 \pm 0.02^{+0.05}_{-0.03}$
-0.7 – -0.4	$1.534 \pm 0.019^{+0.036}_{-0.039}$	$1.51 \pm 0.02^{+0.03}_{-0.02}$	$1.44 \pm 0.02^{+0.06}_{-0.02}$
-0.4 – -0.1	$1.80 \pm 0.02^{+0.05}_{-0.02}$	$1.75 \pm 0.02^{+0.05}_{-0.02}$	$1.68 \pm 0.03^{+0.09}_{-0.03}$
-0.1 – 0.2	$1.97 \pm 0.02^{+0.06}_{-0.02}$	$1.96 \pm 0.02^{+0.05}_{-0.02}$	$1.93 \pm 0.03^{+0.10}_{-0.03}$
0.2 – 0.5	$2.06 \pm 0.02^{+0.08}_{-0.05}$	$2.07 \pm 0.02^{+0.09}_{-0.03}$	$2.19 \pm 0.03^{+0.08}_{-0.05}$
0.5 – 0.8	$2.11 \pm 0.02^{+0.10}_{-0.04}$	$2.17 \pm 0.02^{+0.11}_{-0.02}$	$2.24 \pm 0.03^{+0.12}_{-0.03}$
0.8 – 1.1	$2.17 \pm 0.02^{+0.10}_{-0.04}$	$2.28 \pm 0.02^{+0.13}_{-0.03}$	$2.30 \pm 0.03^{+0.11}_{-0.06}$
1.1 – 1.4	$2.24 \pm 0.03^{+0.08}_{-0.03}$	$2.33 \pm 0.03^{+0.10}_{-0.04}$	$2.48 \pm 0.03^{+0.12}_{-0.06}$
1.4 – 1.7	$2.18 \pm 0.03^{+0.10}_{-0.03}$	$2.36 \pm 0.03^{+0.10}_{-0.05}$	$2.56 \pm 0.03^{+0.16}_{-0.07}$

Table 17. The charged-particle density, $1/N\ dn^{\pm}/d\eta^{\text{Breit}}$, for $50 < Q^2 < 60\,\text{GeV}^2$ and 3 bins in W. The first uncertainty is statistical, the second systematic.

η^{Breit}	$80 < W < 120\,\text{GeV}$	$120 < W < 160\,\text{GeV}$	$160 < W < 200\,\text{GeV}$
-3.1 – -2.8	$0.049 \pm 0.003^{+0.005}_{-0.004}$	$0.044 \pm 0.003^{+0.004}_{-0.004}$	$0.039 \pm 0.003^{+0.004}_{-0.005}$
-2.8 – -2.5	$0.083 \pm 0.004^{+0.008}_{-0.003}$	$0.089 \pm 0.005^{+0.007}_{-0.010}$	$0.064 \pm 0.004^{+0.008}_{-0.004}$
-2.5 – -2.2	$0.149 \pm 0.005^{+0.010}_{-0.006}$	$0.136 \pm 0.006^{+0.009}_{-0.005}$	$0.118 \pm 0.006^{+0.007}_{-0.006}$
-2.2 – -1.9	$0.242 \pm 0.006^{+0.008}_{-0.004}$	$0.242 \pm 0.008^{+0.009}_{-0.012}$	$0.194 \pm 0.007^{+0.013}_{-0.007}$
-1.9 – -1.6	$0.405 \pm 0.008^{+0.017}_{-0.010}$	$0.384 \pm 0.009^{+0.017}_{-0.011}$	$0.330 \pm 0.009^{+0.014}_{-0.008}$
-1.6 – -1.3	$0.607 \pm 0.010^{+0.021}_{-0.008}$	$0.576 \pm 0.011^{+0.006}_{-0.018}$	$0.495 \pm 0.011^{+0.021}_{-0.008}$
-1.3 – -1.0	$0.912 \pm 0.013^{+0.017}_{-0.013}$	$0.815 \pm 0.013^{+0.025}_{-0.014}$	$0.766 \pm 0.014^{+0.024}_{-0.014}$
-1.0 – -0.7	$1.176 \pm 0.014^{+0.029}_{-0.007}$	$1.121 \pm 0.015^{+0.018}_{-0.022}$	$1.029 \pm 0.016^{+0.031}_{-0.011}$
-0.7 – -0.4	$1.461 \pm 0.015^{+0.036}_{-0.014}$	$1.416 \pm 0.017^{+0.016}_{-0.037}$	$1.39 \pm 0.02^{+0.03}_{-0.02}$
-0.4 – -0.1	$1.710 \pm 0.017^{+0.050}_{-0.017}$	$1.649 \pm 0.018^{+0.035}_{-0.017}$	$1.67 \pm 0.02^{+0.06}_{-0.01}$
-0.1 – 0.2	$1.901 \pm 0.018^{+0.057}_{-0.026}$	$1.883 \pm 0.019^{+0.056}_{-0.026}$	$1.88 \pm 0.02^{+0.07}_{-0.03}$
0.2 – 0.5	$2.009 \pm 0.018^{+0.067}_{-0.038}$	$2.044 \pm 0.019^{+0.079}_{-0.028}$	$2.08 \pm 0.02^{+0.08}_{-0.03}$
0.5 – 0.8	$2.106 \pm 0.018^{+0.095}_{-0.051}$	$2.14 \pm 0.02^{+0.08}_{-0.04}$	$2.25 \pm 0.02^{+0.10}_{-0.04}$
0.8 – 1.1	$2.187 \pm 0.018^{+0.092}_{-0.032}$	$2.26 \pm 0.02^{+0.11}_{-0.03}$	$2.30 \pm 0.02^{+0.12}_{-0.04}$
1.1 – 1.4	$2.24 \pm 0.02^{+0.08}_{-0.04}$	$2.33 \pm 0.02^{+0.12}_{-0.02}$	$2.39 \pm 0.02^{+0.16}_{-0.04}$
1.4 – 1.7	$2.21 \pm 0.02^{+0.08}_{-0.03}$	$2.40 \pm 0.02^{+0.09}_{-0.04}$	$2.46 \pm 0.02^{+0.15}_{-0.05}$

Table 18. The charged-particle density, $1/N\ dn^{\pm}/d\eta^{\text{Breit}}$, for $40 < Q^2 < 50\,\text{GeV}^2$ and 3 bins in W. The first uncertainty is statistical, the second systematic.

JHEP06(2010)009

η^{Breit}	$80 < W < 120\,\text{GeV}$	$120 < W < 160\,\text{GeV}$	$160 < W < 200\,\text{GeV}$
-3.1 – -2.8	$0.036 \pm 0.002^{+0.003}_{-0.002}$	$0.035 \pm 0.002^{+0.004}_{-0.002}$	$0.029 \pm 0.002^{+0.004}_{-0.003}$
-2.8 – -2.5	$0.066 \pm 0.003^{+0.003}_{-0.003}$	$0.055 \pm 0.003^{+0.005}_{-0.002}$	$0.056 \pm 0.003^{+0.004}_{-0.004}$
-2.5 – -2.2	$0.122 \pm 0.004^{+0.003}_{-0.004}$	$0.108 \pm 0.004^{+0.007}_{-0.004}$	$0.090 \pm 0.004^{+0.008}_{-0.003}$
-2.2 – -1.9	$0.196 \pm 0.005^{+0.007}_{-0.004}$	$0.185 \pm 0.005^{+0.006}_{-0.007}$	$0.160 \pm 0.005^{+0.008}_{-0.006}$
-1.9 – -1.6	$0.344 \pm 0.006^{+0.008}_{-0.008}$	$0.300 \pm 0.006^{+0.006}_{-0.004}$	$0.260 \pm 0.006^{+0.011}_{-0.006}$
-1.6 – -1.3	$0.529 \pm 0.007^{+0.011}_{-0.008}$	$0.488 \pm 0.008^{+0.010}_{-0.011}$	$0.431 \pm 0.008^{+0.024}_{-0.009}$
-1.3 – -1.0	$0.767 \pm 0.009^{+0.006}_{-0.010}$	$0.696 \pm 0.009^{+0.016}_{-0.009}$	$0.653 \pm 0.010^{+0.020}_{-0.010}$
-1.0 – -0.7	$1.050 \pm 0.010^{+0.018}_{-0.011}$	$0.964 \pm 0.011^{+0.014}_{-0.008}$	$0.913 \pm 0.012^{+0.045}_{-0.016}$
-0.7 – -0.4	$1.342 \pm 0.011^{+0.031}_{-0.008}$	$1.260 \pm 0.012^{+0.019}_{-0.011}$	$1.228 \pm 0.014^{+0.045}_{-0.014}$
-0.4 – -0.1	$1.597 \pm 0.012^{+0.032}_{-0.017}$	$1.548 \pm 0.014^{+0.024}_{-0.022}$	$1.508 \pm 0.016^{+0.052}_{-0.012}$
-0.1 – 0.2	$1.816 \pm 0.013^{+0.047}_{-0.023}$	$1.795 \pm 0.014^{+0.053}_{-0.026}$	$1.757 \pm 0.016^{+0.067}_{-0.013}$
0.2 – 0.5	$1.973 \pm 0.014^{+0.055}_{-0.019}$	$1.980 \pm 0.015^{+0.086}_{-0.014}$	$2.035 \pm 0.017^{+0.076}_{-0.015}$
0.5 – 0.8	$2.089 \pm 0.014^{+0.091}_{-0.024}$	$2.133 \pm 0.015^{+0.087}_{-0.026}$	$2.168 \pm 0.017^{+0.097}_{-0.026}$
0.8 – 1.1	$2.200 \pm 0.014^{+0.078}_{-0.035}$	$2.229 \pm 0.015^{+0.126}_{-0.019}$	$2.303 \pm 0.018^{+0.117}_{-0.032}$
1.1 – 1.4	$2.268 \pm 0.015^{+0.079}_{-0.031}$	$2.328 \pm 0.016^{+0.129}_{-0.012}$	$2.367 \pm 0.018^{+0.145}_{-0.051}$
1.4 – 1.7	$2.285 \pm 0.017^{+0.069}_{-0.031}$	$2.379 \pm 0.016^{+0.126}_{-0.025}$	$2.473 \pm 0.019^{+0.140}_{-0.032}$

Table 19. The charged-particle density, $1/N\ dn^{\pm}/d\eta^{\text{Breit}}$, for $30 < Q^2 < 40\,\text{GeV}^{\,2}$ and 3 bins in W. The first uncertainty is statistical, the second systematic.

η^{Breit}	$80 < W < 120\,\text{GeV}$	$120 < W < 160\,\text{GeV}$
-3.1 – -2.8	$0.0268 \pm 0.0012^{+0.0016}_{-0.0018}$	$0.0233 \pm 0.0012^{+0.0017}_{-0.0012}$
-2.8 – -2.5	$0.0475 \pm 0.0016^{+0.0031}_{-0.0012}$	$0.0470 \pm 0.0019^{+0.0022}_{-0.0020}$
-2.5 – -2.2	$0.091 \pm 0.002^{+0.003}_{-0.003}$	$0.075 \pm 0.002^{+0.003}_{-0.002}$
-2.2 – -1.9	$0.155 \pm 0.003^{+0.004}_{-0.004}$	$0.130 \pm 0.003^{+0.005}_{-0.003}$
-1.9 – -1.6	$0.256 \pm 0.004^{+0.006}_{-0.005}$	$0.220 \pm 0.004^{+0.006}_{-0.003}$
-1.6 – -1.3	$0.403 \pm 0.005^{+0.007}_{-0.009}$	$0.364 \pm 0.005^{+0.010}_{-0.004}$
-1.3 – -1.0	$0.620 \pm 0.006^{+0.007}_{-0.007}$	$0.543 \pm 0.006^{+0.012}_{-0.004}$
-1.0 – -0.7	$0.863 \pm 0.007^{+0.008}_{-0.012}$	$0.783 \pm 0.007^{+0.009}_{-0.007}$
-0.7 – -0.4	$1.142 \pm 0.008^{+0.010}_{-0.012}$	$1.055 \pm 0.008^{+0.022}_{-0.007}$
-0.4 – -0.1	$1.427 \pm 0.009^{+0.016}_{-0.013}$	$1.370 \pm 0.009^{+0.019}_{-0.007}$
-0.1 – 0.2	$1.692 \pm 0.009^{+0.027}_{-0.018}$	$1.634 \pm 0.010^{+0.037}_{-0.007}$
0.2 – 0.5	$1.882 \pm 0.010^{+0.049}_{-0.017}$	$1.871 \pm 0.010^{+0.064}_{-0.012}$
0.5 – 0.8	$2.049 \pm 0.010^{+0.076}_{-0.018}$	$2.072 \pm 0.011^{+0.074}_{-0.017}$
0.8 – 1.1	$2.177 \pm 0.010^{+0.091}_{-0.021}$	$2.265 \pm 0.012^{+0.105}_{-0.023}$
1.1 – 1.4	$2.269 \pm 0.011^{+0.077}_{-0.032}$	$2.365 \pm 0.012^{+0.115}_{-0.015}$
1.4 – 1.7	$2.290 \pm 0.011^{+0.067}_{-0.017}$	$2.429 \pm 0.012^{+0.120}_{-0.028}$

Table 20. The charged-particle density, $1/N\ dn^{\pm}/d\eta^{\text{Breit}}$, for $20 < Q^2 < 30\,\text{GeV}^{\,2}$ and 2 bins in W. The first uncertainty is statistical, the second systematic.

JHEP06(2010)009

$\eta^{\rm Breit}$			$80 < W < 120\,\text{GeV}$	$120 < W < 160\,\text{GeV}$
-3.1	–	-2.8	$0.0156 \pm 0.0006\ ^{+0.0002}_{-0.0007}$	$0.0138 \pm 0.0006^{+0.0006}_{-0.0007}$
-2.8	–	-2.5	$0.0300 \pm 0.0008^{+0.0007}_{-0.0013}$	$0.0252 \pm 0.0008^{+0.0012}_{-0.0014}$
-2.5	–	-2.2	$0.0548 \pm 0.0011^{+0.0023}_{-0.0020}$	$0.0458 \pm 0.0011^{+0.0019}_{-0.0019}$
-2.2	–	-1.9	$0.0915 \pm 0.0014^{+0.0015}_{-0.0024}$	$0.0785 \pm 0.0014^{+0.0020}_{-0.0027}$
-1.9	–	-1.6	$0.1564 \pm 0.0019^{+0.0026}_{-0.0034}$	$0.1327 \pm 0.0018^{+0.0024}_{-0.0032}$
-1.6	–	-1.3	$0.260 \pm 0.002^{+0.003}_{-0.005}$	$0.223 \pm 0.002^{+0.005}_{-0.007}$
-1.3	–	-1.0	$0.404 \pm 0.003^{+0.005}_{-0.009}$	$0.354 \pm 0.003^{+0.006}_{-0.009}$
-1.0	–	-0.7	$0.591 \pm 0.003^{+0.005}_{-0.010}$	$0.529 \pm 0.004^{+0.011}_{-0.012}$
-0.7	–	-0.4	$0.827 \pm 0.004^{+0.007}_{-0.013}$	$0.769 \pm 0.004^{+0.013}_{-0.022}$
-0.4	–	-0.1	$1.100 \pm 0.005^{+0.015}_{-0.016}$	$1.051 \pm 0.005^{+0.017}_{-0.024}$
-0.1	–	0.2	$1.409 \pm 0.005^{+0.013}_{-0.016}$	$1.369 \pm 0.006^{+0.024}_{-0.027}$
0.2	–	0.5	$1.665 \pm 0.006^{+0.032}_{-0.018}$	$1.667 \pm 0.006^{+0.042}_{-0.010}$
0.5	–	0.8	$1.900 \pm 0.006^{+0.050}_{-0.016}$	$1.929 \pm 0.007^{+0.066}_{-0.009}$
0.8	–	1.1	$2.086 \pm 0.007^{+0.069}_{-0.014}$	$2.132 \pm 0.007^{+0.099}_{-0.011}$
1.1	–	1.4	$2.202 \pm 0.007^{+0.086}_{-0.015}$	$2.304 \pm 0.008^{+0.101}_{-0.016}$
1.4	–	1.7	$2.259 \pm 0.007^{+0.081}_{-0.021}$	$2.395 \pm 0.008^{+0.138}_{-0.013}$

Table 21. The charged-particle density, $1/N\ dn^{\pm}/d\eta^{\rm Breit}$, for $10 < Q^2 < 20\,\text{GeV}^{\,2}$ and 2 bins in W. The first uncertainty is statistical, the second systematic.

Author list

H. Abramowicz,[44,ad] **I. Abt,**[34] **L. Adamczyk,**[13] **M. Adamus,**[53] **S. Antonelli,**[4] **P. Antonioli,**[3] **A. Antonov,**[32] **M. Arneodo,**[49] **V. Aushev,**[26,x] **Y. Aushev,**[26,x] **O. Bachynska,**[15] **A. Bamberger,**[19] **A.N. Barakbaev,**[25] **G. Barbagli,**[17] **G. Bari,**[3] **F. Barreiro,**[29] **D. Bartsch,**[5] **M. Basile,**[4] **O. Behnke,**[15] **J. Behr,**[15] **U. Behrens,**[15] **L. Bellagamba,**[3] **A. Bertolin,**[38] **S. Bhadra,**[56] **M. Bindi,**[4] **C. Blohm,**[15] **T. Bołd,**[13] **E.G. Boos,**[25] **M. Borodin,**[26] **K. Borras,**[15] **D. Boscherini,**[3] **D. Bot,**[15] **S.K. Boutle,**[51] **I. Brock,**[5] **E. Brownson,**[55] **R. Brugnera,**[39] **N. Brümmer,**[36] **A. Bruni,**[3] **G. Bruni,**[3] **B. Brzozowska,**[52] **P.J. Bussey,**[20] **J.M. Butterworth,**[51] **B. Bylsma,**[36] **A. Caldwell,**[34] **M. Capua,**[8] **R. Carlin,**[39] **C.D. Catterall,**[56] **S. Chekanov,**[1] **J. Chwastowski,**[12] **J. Ciborowski,**[52,ai] **R. Ciesielski,**[15] **L. Cifarelli,**[4] **F. Cindolo,**[3] **A. Contin,**[4] **A.M. Cooper-Sarkar,**[37] **N. Coppola,**[15,j] **M. Corradi,**[3] **F. Corriveau,**[30] **M. Costa,**[48] **G. D'Agostini,**[42] **F. Dal Corso,**[38] **J. de Favereau,**[28] **J. del Peso,**[29] **R.K. Dementiev,**[33] **S. De Pasquale,**[4,b] **M. Derrick,**[1] **R.C.E. Devenish,**[37] **D. Dobur,**[19] **B.A. Dolgoshein,**[32] **A.T. Doyle,**[20] **V. Drugakov,**[16] **L.S. Durkin,**[36] **S. Dusini,**[38] **Y. Eisenberg,**[54] **P.F. Ermolov ,**[33,†] **A. Eskreys,**[12] **S. Fang,**[15] **S. Fazio,**[8] **J. Ferrando,**[37] **M.I. Ferrero,**[48] **J. Figiel,**[12] **M. Forrest,**[20] **S. Fourletov,**[50,ah] **A. Galas,**[12] **E. Gallo,**[17] **A. Garfagnini,**[39] **A. Geiser,**[15] **I. Gialas,**[21,t] **L.K. Gladilin,**[33] **D. Gladkov,**[32] **C. Glasman,**[29] **O. Gogota,**[26] **Yu.A. Golubkov,**[33] **P. Göttlicher,**[15,k] **I. Grabowska-Bołd,**[13] **J. Grebenyuk,**[15] **I. Gregor,**[15] **G. Grigorescu,**[35] **G. Grzelak,**[52] **C. Gwenlan,**[37,aa] **T. Haas,**[15] **W. Hain,**[15] **R. Hamatsu,**[47] **J.C. Hart,**[43]

JHEP06(2010)009

H. Hartmann,[5] G. Hartner,[56] E. Hilger,[5] D. Hochman,[54] U. Holm,[22] R. Hori,[46] K. Horton,[37,ab] A. Hüttmann,[15] Z.A. Ibrahim,[10] Y. Iga,[41] R. Ingbir,[44] M. Ishitsuka,[45] H.-P. Jakob,[5] F. Januschek,[15] M. Jimenez,[29] T.W. Jones,[51] M. Jüngst,[5] I. Kadenko,[26] B. Kahle,[15] B. Kamaluddin,[10] S. Kananov,[44] T. Kanno,[45] U. Karshon,[54] F. Karstens,[19] I.I. Katkov,[15,l] M. Kaur,[7] P. Kaur,[7,d] A. Keramidas,[35] L.A. Khein,[33] J.Y. Kim,[9,f] D. Kisielewska,[13] S. Kitamura,[47,ae] R. Klanner,[22] U. Klein,[15,m] E. Koffeman,[35] D. Kollar,[34] P. Kooijman,[35] Ie. Korol,[26] A. Kotański,[14,h] U. Kötz,[15] H. Kowalski,[15] P. Kulinski,[52] O. Kuprash,[26] M. Kuze,[45] V.A. Kuzmin,[33] A. Lee,[36] B.B. Levchenko,[33,y] A. Levy,[44] V. Libov,[15] S. Limentani,[39] T.Y. Ling,[36] M. Lisovyi,[15] W. Lohmann,[16] B. Löhr,[15] E. Lohrmann,[22] J.H. Loizides,[51] K.R. Long,[23] A. Longhin,[38] D. Lontkovskyi,[26] J. Łukasik,[13,g] O.Yu. Lukina,[33] P. Łużniak,[52,aj] J. Maeda,[45] S. Magill,[1] I. Makarenko,[26] J. Malka,[52,aj] R. Mankel,[15,n] A. Margotti,[3] G. Marini,[42] J.F. Martin,[50] A. Mastroberardino,[8] T. Matsumoto,[24,u] M.C.K. Mattingly,[2] F. Mohamad Idris,[10] V. Monaco,[48] A. Montanari,[15] J.D. Morris,[6,c] B. Musgrave,[1] K. Nagano,[24] T. Namsoo,[15] R. Nania,[3] D. Nicholass,[1,a] A. Nigro,[42] Y. Ning,[11] U. Noor,[56] D. Notz,[15] R.J. Nowak,[52] B.Y. Oh,[40] N. Okazaki,[46] K. Oliver,[37] K. Olkiewicz,[12] O. Ota,[47,af] K. Papageorgiu,[21] E. Paul,[5] J.M. Pawlak,[52] B. Pawlik,[12] P. G. Pelfer,[18] A. Pellegrino,[35] W. Perlanski,[52,aj] H. Perrey,[22] K. Piotrzkowski,[28] P. Plucinski,[53,ak] N.S. Pokrovskiy,[25] A. Polini,[3] A.S. Proskuryakov,[33] A. Raval,[15] D.D. Reeder,[55] B. Reisert,[34] Z. Ren,[11] Y.D. Ri,[47,ag] A. Robertson,[37] P. Roloff,[15] E. Ron,[29] I. Rubinsky,[15] M. Ruspa,[49] R. Sacchi,[48] A. Salii,[26] U. Samson,[5] G. Sartorelli,[4] A.A. Savin,[55] D.H. Saxon,[20] M. Schioppa,[8] P. Schleper,[22] W.B. Schmidke,[34] V. Schönberg,[5] J. Schwartz,[30] F. Sciulli,[11] L.M. Shcheglova,[33] R. Shehzadi,[5] S. Shimizu,[46,z] I. Singh,[7,d] I.O. Skillicorn,[20] W. Słomiński,[14,i] W.H. Smith,[55] V. Sola,[48] A. Solano,[48] A. Solomin,[6] D. Son,[27] V. Sosnovtsev,[32] A. Spiridonov,[15,o] H. Stadie,[22] L. Stanco,[38] A. Stern,[44] T.P. Stewart,[50] A. Stifutkin,[32] P. Stopa,[12] S. Suchkov,[32] G. Susinno,[8] L. Suszycki,[13] J. Sztuk,[22] D. Szuba,[15,p] J. Szuba,[15,q] A.D. Tapper,[23] E. Tassi,[8,e] J. Terrón,[29] T. Theedt,[15] H. Tiecke,[35] K. Tokushuku,[24,v] O. Tomalak,[26] J. Tomaszewska,[15,r] T. Tsurugai,[31] M. Turcato,[22] T. Tymieniecka,[53,al] M. Vázquez,[35,z] A. Verbytskyi,[15] V. Viazlo,[26] N.N. Vlasov,[19,s] O. Volynets,[26] R. Walczak,[37] W.A.T. Wan Abdullah,[10] J.J. Whitmore,[40,ac] J. Whyte,[56] M. Wing,[51] M. Wlasenko,[5] G. Wolf,[15] H. Wolfe,[55] K. Wrona,[15] S. Yamada,[24] Y. Yamazaki,[24,w] R. Yoshida,[1] C. Youngman,[15] A.F. Żarnecki,[52] O. Zenaiev,[26] B.O. Zhautykov,[25] N. Zhmak,[26,x] C. Zhou,[30] A. Zichichi,[4] M. Zolko[26] and D.S. Zotkin[33]

[1] *Argonne National Laboratory,*
Argonne, Illinois 60439-4815, U.S.A.[A]
[2] *Andrews University,*
Berrien Springs, Michigan 49104-0380, U.S.A.

JHEP06(2010)009

[3] *INFN Bologna, Bologna, Italy*[B]
[4] *University and INFN Bologna, Bologna, Italy*[B]
[5] *Physikalisches Institut der Universität Bonn, Bonn, Germany*[C]
[6] *H.H. Wills Physics Laboratory, University of Bristol, Bristol, U.K.*[D]
[7] *Panjab University, Department of Physics, Chandigarh, India*
[8] *Calabria University, Physics Department and INFN, Cosenza, Italy*[B]
[9] *Chonnam National University, Kwangju, South Korea*
[10] *Jabatan Fizik, Universiti Malaya, 50603 Kuala Lumpur, Malaysia*[E]
[11] *Nevis Laboratories, Columbia University, Irvington on Hudson, New York 10027, U.S.A.*[F]
[12] *The Henryk Niewodniczanski Institute of Nuclear Physics, Polish Academy of Sciences, Cracow, Poland*[G]
[13] *Faculty of Physics and Applied Computer Science, AGH-University of Science and Technology, Cracow, Poland*[H]
[14] *Department of Physics, Jagellonian University, Cracow, Poland*
[15] *Deutsches Elektronen-Synchrotron DESY, Hamburg, Germany*
[16] *Deutsches Elektronen-Synchrotron DESY, Zeuthen, Germany*
[17] *INFN Florence, Florence, Italy*[B]
[18] *University and INFN Florence, Florence, Italy*[B]
[19] *Fakultät für Physik der Universität Freiburg i.Br., Freiburg i.Br., Germany*[C]
[20] *Department of Physics and Astronomy, University of Glasgow, Glasgow, U.K.*[D]
[21] *Department of Engineering in Management and Finance, Univ. of the Aegean, Chios, Greece*
[22] *Hamburg University, Institute of Exp. Physics, Hamburg, Germany*[C]

JHEP06(2010)009

[23] *Imperial College London, High Energy Nuclear Physics Group, London, U.K.*[D]
[24] *Institute of Particle and Nuclear Studies, KEK, Tsukuba, Japan*[I]
[25] *Institute of Physics and Technology of Ministry of Education and Science of Kazakhstan, Almaty, Kazakhstan*
[26] *Institute for Nuclear Research, National Academy of Sciences and Kiev National University, Kiev, Ukraine*
[27] *Kyungpook National University, Center for High Energy Physics, Daegu, South Korea*[J]
[28] *Institut de Physique Nucléaire, Université Catholique de Louvain, Louvain-la-Neuve, Belgium*[K]
[29] *Departamento de Física Teórica, Universidad Autónoma de Madrid, Madrid, Spain*[L]
[30] *Department of Physics, McGill University, Montréal, Québec, H3A 2T8 Canada*[M]
[31] *Meiji Gakuin University, Faculty of General Education, Yokohama, Japan*[I]
[32] *Moscow Engineering Physics Institute, Moscow, Russia*[N]
[33] *Moscow State University, Institute of Nuclear Physics, Moscow, Russia*[O]
[34] *Max-Planck-Institut für Physik, München, Germany*
[35] *NIKHEF and University of Amsterdam, Amsterdam, Netherlands*[P]
[36] *Physics Department, Ohio State University, Columbus, Ohio 43210, U.S.A.*[A]
[37] *Department of Physics, University of Oxford, Oxford, U.K.*[D]
[38] *INFN Padova, Padova, Italy*[B]
[39] *Dipartimento di Fisica dell' Università and INFN, Padova, Italy*[B]
[40] *Department of Physics, Pennsylvania State University, University Park, Pennsylvania 16802, U.S.A.*[F]
[41] *Polytechnic University, Sagamihara, Japan*[I]
[42] *Dipartimento di Fisica, Università 'La Sapienza' and INFN, Rome, Italy*[e]
[43] *Rutherford Appleton Laboratory, Chilton, Didcot, Oxon, U.K.*[D]

JHEP06(2010)009

[44] *Raymond and Beverly Sackler Faculty of Exact Sciences, School of Physics, Tel Aviv University, Tel Aviv, Israel*[Q]
[45] *Department of Physics, Tokyo Institute of Technology, Tokyo, Japan*[I]
[46] *Department of Physics, University of Tokyo, Tokyo, Japan*[I]
[47] *Tokyo Metropolitan University, Department of Physics, Tokyo, Japan*[I]
[48] *Università di Torino and INFN, Torino, Italy*[B]
[49] *Università del Piemonte Orientale, Novara, and INFN, Torino, Italy*[B]
[50] *Department of Physics, University of Toronto, Toronto, Ontario, M5S 1A7 Canada*[M]
[51] *Physics and Astronomy Department, University College London, London, U.K.*[D]
[52] *Warsaw University, Institute of Experimental Physics, Warsaw, Poland*
[53] *Institute for Nuclear Studies, Warsaw, Poland*
[54] *Department of Particle Physics, Weizmann Institute, Rehovot, Israel*[R]
[55] *Department of Physics, University of Wisconsin, Madison, Wisconsin 53706, U.S.A.*[A]
[56] *Department of Physics, York University, Ontario, M3J1P3 Canada*[M]

[A] *supported by the U.S. Department of Energy*
[B] *supported by the Italian National Institute for Nuclear Physics (INFN)*
[C] *supported by the German Federal Ministry for Education and Research (BMBF), under contract Nos. 05 HZ6PDA, 05 HZ6GUA, 05 HZ6VFA and 05 HZ4KHA*
[D] *supported by the Science and Technology Facilities Council, U.K.*
[E] *supported by an FRGS grant from the Malaysian government*
[F] *supported by the U.S. National Science Foundation. Any opinion, findings and conclusions or recommendations expressed in this material are those of the authors and do not necessarily reflect the views of the National Science Foundation.*
[G] *supported by the Polish State Committee for Scientific Research, project No. DESY/256/2006 - 154/DES/2006/03*
[H] *supported by the Polish Ministry of Science and Higher Education as a scientific project (2009-2010)*
[I] *supported by the Japanese Ministry of Education, Culture, Sports, Science and Technology (MEXT) and its grants for Scientific Research*

JHEP06(2010)009

[J] supported by the Korean Ministry of Education and Korea Science and Engineering Foundation
[K] supported by FNRS and its associated funds (IISN and FRIA) and by an Inter-University Attraction Poles Programme subsidised by the Belgian Federal Science Policy Office
[L] supported by the Spanish Ministry of Education and Science through funds provided by CICYT
[M] supported by the Natural Sciences and Engineering Research Council of Canada (NSERC)
[N] partially supported by the German Federal Ministry for Education and Research (BMBF)
[O] supported by RF Presidential grant N 1456.2008.2 for the leading scientific schools and by the Russian Ministry of Education and Science through its grant for Scientific Research on High Energy Physics
[P] supported by the Netherlands Foundation for Research on Matter (FOM)
[Q] supported by the Israel Science Foundation
[R] supported in part by the MINERVA Gesellschaft für Forschung GmbH, the Israel Science Foundation (grant No. 293/02-11.2) and the U.S.-Israel Binational Science Foundation
[a] also affiliated with University College London, U.K.
[b] now at University of Salerno, Italy
[c] now at Queen Mary University of London, U.K.
[d] also working at Max Planck Institute, Munich, Germany
[e] also Senior Alexander von Humboldt Research Fellow at Hamburg University, Institute of Experimental Physics, Hamburg, Germany
[f] supported by Chonnam National University, South Korea, in 2009
[g] now at Institute of Aviation, Warsaw, Poland
[h] supported by the research grant No. 1 P03B 04529 (2005-2008)
[i] This work was supported in part by the Marie Curie Actions Transfer of Knowledge project COCOS (contract MTKD-CT-2004-517186)
[j] now at DESY group FS-CFEL-1
[k] now at DESY group FEB, Hamburg, Germany
[l] also at Moscow State University, Russia
[m] now at University of Liverpool, U.K.
[n] on leave of absence at CERN, Geneva, Switzerland
[o] also at Institute of Theoretical and Experimental Physics, Moscow, Russia
[p] also at INP, Cracow, Poland
[q] also at FPACS, AGH-UST, Cracow, Poland
[r] partially supported by Warsaw University, Poland
[s] partially supported by Moscow State University, Russia
[t] also affiliated with DESY, Germany
[u] now at Japan Synchrotron Radiation Research Institute (JASRI), Hyogo, Japan
[v] also at University of Tokyo, Japan
[w] now at Kobe University, Japan
[x] supported by DESY, Germany
[y] partially supported by Russian Foundation for Basic Research grant No. 05-02-39028-NSFC-a

JHEP06(2010)009

[z] now at CERN, Geneva, Switzerland
[†] deceased
[aa] STFC Advanced Fellow
[ab] nee Korcsak-Gorzo
[ac] This material was based on work supported by the National Science Foundation, while working at the Foundation.
[ad] also at Max Planck Institute, Munich, Germany, Alexander von Humboldt Research Award
[ae] now at Nihon Institute of Medical Science, Japan
[af] now at SunMelx Co. Ltd., Tokyo, Japan
[ag] now at Osaka University, Osaka, Japan
[ah] now at University of Bonn, Germany
[ai] also at Łódź University, Poland
[aj] member of Łódź University, Poland
[ak] now at Lund University, Lund, Sweden
[al] also at University of Podlasie, Siedlce, Poland

References

[1] ZEUS collaboration, M. Derrick et al., *Measurement of multiplicity and momentum spectra in the current fragmentation region of the Breit frame at HERA*, *Z. Phys.* **C 67** (1995) 93 [hep-ex/9501012] [SPIRES].

[2] ZEUS collaboration, J. Breitweg et al., *Observation of scaling violations in scaled momentum distributions at HERA*, *Phys. Lett.* **B 414** (1997) 428 [hep-ex/9710011] [SPIRES].

[3] ZEUS collaboration, J. Breitweg et al., *Measurement of multiplicity and momentum spectra in the current and target regions of the Breit frame in deep inelastic scattering at HERA*, *Eur. Phys. J.* **C 11** (1999) 251 [hep-ex/9903056] [SPIRES].

[4] H1 collaboration, F.D. Aaron et al., *Charged particle production in high Q2 deep-inelastic scattering at HERA*, *Phys. Lett.* **B 654** (2007) 148 [arXiv:0706.2456] [SPIRES].

[5] G. Altarelli, R.K. Ellis, G. Martinelli and S.-Y. Pi, *Processes involving fragmentation functions beyond the leading order in QCD*, *Nucl. Phys.* **B 160** (1979) 301 [SPIRES].

[6] P. Nason and B.R. Webber, *Scaling violation in e^+e^- fragmentation functions: QCD evolution, hadronization and heavy quark mass effects*, *Nucl. Phys.* **B 421** (1994) 473 [*Erratum ibid.* **B 480** (1996) 755] [SPIRES].

[7] C.P. Fong and B.R. Webber, *Higher order QCD corrections to hadron energy distributions in jets*, *Phys. Lett.* **B 229** (1989) 289 [SPIRES].

[8] C.P. Fong and B.R. Webber, *One and two particle distributions at small x in QCD jets*, *Nucl. Phys.* **B 355** (1991) 54 [SPIRES].

JHEP06(2010)009

[9] Y.L. Dokshitzer, V.A. Khoze and S.I. Troian, *Inclusive particle spectra from QCD cascades*, *Int. J. Mod. Phys.* **A 7** (1992) 1875 [SPIRES].

[10] Y.I. Dokshitzer et al., *Basics of perturbative QCD*, Editions Frontiéres, Gif-sur-Yvette France (1991), pg. 169.

[11] Y.I. Azimov, Y.L. Dokshitzer, V.A. Khoze and S.I. Troyan, *Similarity of parton and hadron spectra in QCD jets*, *Z. Phys.* **C 27** (1985) 65 [SPIRES].

[12] S. Kretzer, *Fragmentation functions from flavour-inclusive and flavour-tagged e^+e^- annihilations*, *Phys. Rev.* **D 62** (2000) 054001 [hep-ph/0003177] [SPIRES].

[13] B.A. Kniehl, G. Kramer and B. Pötter, *Strong coupling constant from scaling violations in fragmentation functions*, *Phys. Rev. Lett.* **85** (2000) 5288 [hep-ph/0003297] [SPIRES].

[14] S. Albino, B.A. Kniehl and G. Kramer, *Fragmentation functions for light charged hadrons with complete quark flavour separation*, *Nucl. Phys.* **B 725** (2005) 181 [hep-ph/0502188] [SPIRES].

[15] S. Albino, B.A. Kniehl and G. Kramer, *AKK update: improvements from new theoretical input and experimental data*, *Nucl. Phys.* **B 803** (2008) 42 [arXiv:0803.2768] [SPIRES].

[16] D. de Florian, R. Sassot and M. Stratmann, *Global analysis of fragmentation functions for pions and kaons and their uncertainties*, *Phys. Rev.* **D 75** (2007) 114010 [hep-ph/0703242] [SPIRES].

[17] D. de Florian, R. Sassot and M. Stratmann, *Global analysis of fragmentation functions for protons and charged hadrons*, *Phys. Rev.* **D 76** (2007) 074033 [arXiv:0707.1506] [SPIRES].

[18] V.A. Khoze and W. Ochs, *Perturbative QCD approach to multiparticle production*, *Int. J. Mod. Phys.* **A 12** (1997) 2949 [hep-ph/9701421] [SPIRES].

[19] V.A. Khoze, S. Lupia and W. Ochs, *Perturbative description of particle spectra at LEP-1.5*, *Phys. Lett.* **B 386** (1996) 451 [hep-ph/9604410] [SPIRES].

[20] A. Petersen et al., *Multi-hadronic events at $E_{\rm c.m.} = 29\ GeV$ and predictions of QCD models from $E_{\rm c.m.} = 29\ GeV$ to $E_{\rm c.m.} = 93\ GeV$*, *Phys. Rev.* **D 37** (1988) 1 [SPIRES].

[21] TASSO collaboration, W. Braunschweig et al., *Global jet properties at 14 GeV to 44 GeV center-of-mass energy in e^+e^- annihilation*, *Z. Phys.* **C 47** (1990) 187 [SPIRES].

[22] AMY collaboration, Y.K. Li et al., *Multi-hadron event properties in e^+e^- annihilation at $\sqrt{s} = 52\ GeV$ to 57 GeV*, *Phys. Rev.* **D 41** (1990) 2675 [SPIRES].

[23] DELPHI collaboration, P. Abreu et al., *Determination of α_s from the scaling violation in the fragmentation functions in e^+e^- annihilation*, *Phys. Lett.* **B 311** (1993) 408 [SPIRES].

[24] ZEUS collaboration, S. Chekanov et al., *Energy dependence of the charged multiplicity in deep inelastic scattering at HERA*, *JHEP* **06** (2008) 061 [arXiv:0803.3878] [SPIRES].

[25] J. Benecke et al., *Hypothesis of limiting fragmentation in high-energy collisions*, *Phys. Rev.* **188** (1969) 2159 [SPIRES].

[26] PHOBOS collaboration, B.B. Back et al., *Charged-particle pseudorapidity distributions in Au+Au collisions at $s_{NN}^{1/2} = 62.4\ GeV$*, *Phys. Rev.* **C 74** (2006) 021901 [nucl-ex/0509034] [SPIRES].

[27] STAR collaboration, J. Adams et al., *Multiplicity and pseudorapidity distributions of charged particles and photons at forward pseudorapidity in Au + Au collisions at $s_{NN}^{1/2} = 62.4\ GeV$*, *Phys. Rev.* **C 73** (2006) 034906 [nucl-ex/0511026] [SPIRES].

JHEP06(2010)009

[28] PHOBOS collaboration, B.B. Back et al., *The significance of the fragmentation region in ultrarelativistic heavy ion collisions*, *Phys. Rev. Lett.* **91** (2003) 052303 [nucl-ex/0210015] [SPIRES].

[29] BRAHMS collaboration, I.G. Bearden et al., *Pseudorapidity distributions of charged particles from Au+Au collisions at the maximum RHIC energy*, *Phys. Rev. Lett.* **88** (2002) 202301 [nucl-ex/0112001] [SPIRES].

[30] BRAHMS collaboration, I.G. Bearden et al., *Charged particle densities from Au + Au collisions at* $s_{NN}^{1/2} = 130$ *GeV*, *Phys. Lett.* **B 523** (2001) 227 [nucl-ex/0108016] [SPIRES].

[31] ZEUS collaboration, U. Holm ed., *The ZEUS detector*, status report, unpublished, available on http://www-zeus.desy.de/bluebook/bluebook.html, DESY Germany (1993).

[32] N. Harnew et al., *Vertex triggering using time difference measurements in the ZEUS central tracking detector*, *Nucl. Instrum. Meth.* **A 279** (1989) 290 [SPIRES].

[33] B. Foster et al., *The performance of the ZEUS central tracking detector z-by-timing electronics in a transputer based data acquisition system*, *Nucl. Phys. (Proc. Suppl.)* **B 32** (1993) 181 [SPIRES].

[34] ZEUS collaboration, B. Foster et al., *The design and construction of the ZEUS central tracking detector*, *Nucl. Instrum. Meth.* **A 338** (1994) 254 [SPIRES].

[35] ZEUS collaboration, A. Polini et al., *The design and performance of the ZEUS micro vertex detector*, *Nucl. Instrum. Meth.* **A 581** (2007) 656 [arXiv:0708.3011] [SPIRES].

[36] M. Derrick et al., *Design and construction of the ZEUS barrel calorimeter*, *Nucl. Instrum. Meth.* **A 309** (1991) 77 [SPIRES].

[37] ZEUS Calorimeter Group collaboration, A. Andresen et al., *Construction and beam test of the ZEUS forward and rear calorimeter*, *Nucl. Instrum. Meth.* **A 309** (1991) 101 [SPIRES].

[38] A. Caldwell et al., *Design and implementation of a high precision readout system for the ZEUS calorimeter*, *Nucl. Instrum. Meth.* **A 321** (1992) 356 [SPIRES].

[39] ZEUS Barrel Calorimeter Group collaboration, A. Bernstein et al., *Beam tests of the ZEUS barrel calorimeter*, *Nucl. Instrum. Meth.* **A 336** (1993) 23 [SPIRES].

[40] ZEUS collaboration, A. Bamberger et al., *The small angle rear tracking detector of ZEUS*, *Nucl. Instrum. Meth.* **A 401** (1997) 63 [SPIRES].

[41] ZEUS Presampler Group collaboration, A. Bamberger et al., *The presampler for the forward and rear calorimeter in the ZEUS detector*, *Nucl. Instrum. Meth.* **A 382** (1996) 419 [hep-ex/9609006] [SPIRES].

[42] ZEUS Luminosity Group collaboration, J. Andruszków et al., *First measurement of HERA luminosity by ZEUS lumi monitor*, preprint DESY-92-066, DESY, Germany (1992) [SPIRES].

[43] ZEUS collaboration, M. Derrick et al., *Measurement of total and partial photon proton cross-sections at* 180 *GeV center-of-mass energy*, *Z. Phys.* **C 63** (1994) 391 [SPIRES].

[44] ZEUS Luminosity Group collaboration, J. Andruszkow et al., *Luminosity measurement in the ZEUS experiment*, *Acta Phys. Polon.* **B 32** (2001) 2025 [SPIRES].

[45] M. Helbich et al., *The spectrometer system for measuring ZEUS luminosity at HERA*, *Nucl. Instrum. Meth.* **A 565** (2006) 572 [physics/0512153] [SPIRES].

JHEP06(2010)009

[46] W.H. Smith, K. Tokushuku and L.W. Wiggers, *The ZEUS trigger system*, in *Proceedings of Computing in High Energy Physics (CHEP 92)*, Annecy France September 21–25 1992, C. Verkerk and W. Wojcik eds., CERN, Geneva Switzerland (1992), pg. 222 [DESY-92-150B] [SPIRES].

[47] P.D. Allfrey et al., *The design and performance of the ZEUS global tracking trigger*, *Nucl. Instrum. Meth.* **A 580** (2007) 1257 [SPIRES].

[48] H. Abramowicz, A. Caldwell and R. Sinkus, *Neural network based electron identification in the ZEUS calorimeter*, *Nucl. Instrum. Meth.* **A 365** (1995) 508 [hep-ex/9505004] [SPIRES].

[49] S. Bentvelsen, J. Engelen and P. Kooijman, *Reconstruction of (x, Q^2) and extraction of structure functions in neutral current scattering at HERA*, in *Proceedings of Workshop on Physics at HERA*, W. Buchmüller and G. Ingelman eds., volume 1, DESY, Hamburg Germany (1992) [NIKHEF-H-92-02] [SPIRES].

[50] B. Brzozowska, *Scaled momentum spectra in deep inelastic scattering at HERA*, thesis, to be published, University of Warsaw, Warsaw Poland (2010).

[51] F. Jacquet and A. Blondel, *Detection of the charged current event — method II*, in *Proceedings of the Study for an ep Facility for Europe*, U. Amaldi ed., Hamburg Germany (1979), pg. 391 [DESY-79-48] [SPIRES].

[52] S. Albino, B.A. Kniehl, G. Kramer and C. Sandoval, *Confronting fragmentation function universality with single hadron inclusive production at HERA and e^+e^- colliders*, *Phys. Rev.* **D 75** (2007) 034018 [hep-ph/0611029] [SPIRES].

[53] A. Bassetto, M. Ciafaloni, G. Marchesini and A.H. Mueller, *Jet multiplicity and soft gluon factorization*, *Nucl. Phys.* **B 207** (1982) 189 [SPIRES].

[54] A.H. Mueller, *Multiplicity and hadron distributions in QCD jets: nonleading terms*, *Nucl. Phys.* **B 213** (1983) 85 [SPIRES].

[55] B.R. Webber, *A QCD model for jet fragmentation including soft gluon interference*, *Nucl. Phys.* **B 238** (1984) 492 [SPIRES].

[56] ZEUS collaboration, S. Chekanov et al., *Scaled momentum distributions of charged particles in dijet photoproduction at HERA*, *JHEP* **08** (2009) 077 [arXiv:0904.3466] [SPIRES].

[57] L. Lönnblad, *ARIADNE version 4: a program for simulation of QCD cascades implementing the color dipole model*, *Comput. Phys. Commun.* **71** (1992) 15 [SPIRES].

[58] G. Gustafson and U. Pettersson, *Dipole formulation of QCD cascades*, *Nucl. Phys.* **B 306** (1988) 746 [SPIRES].

[59] G. Ingelman, A. Edin and J. Rathsman, *LEPTO 6.5 — a Monte Carlo generator for deep inelastic lepton-nucleon scattering*, *Comput. Phys. Commun.* **101** (1997) 108 [hep-ph/9605286] [SPIRES].

[60] K. Charchula, G.A. Schuler and H. Spiesberger, *Combined QED and QCD radiative effects in deep inelastic lepton-proton scattering: the Monte Carlo generator DJANGO6*, *Comput. Phys. Commun.* **81** (1994) 381 [SPIRES].

[61] A. Kwiatkowski, H. Spiesberger and H.J. Möhring, *Heracles: an event generator for e p interactions at HERA energies including radiative processes: version 1.0*, *Comp. Phys. Commun.* **69** (1992) 155 [SPIRES].

JHEP06(2010)009

[62] B. Andersson, G. Gustafson, G. Ingelman and T. Sjöstrand, *Parton fragmentation and string dynamics*, *Phys. Rept.* **97** (1983) 31 [SPIRES].

[63] H.-U. Bengtsson and T. Sjöstrand, *The Lund Monte Carlo for hadronic processes: PYTHIA version* 4.8, *Comput. Phys. Commun.* **46** (1987) 43 [SPIRES].

[64] T. Sjöstrand, *High-energy physics event generation with PYTHIA* 5.7 *and JETSET* 7.4, *Comput. Phys. Commun.* **82** (1994) 74 [SPIRES].

[65] R. Brun et al., GEANT3, technical report CERN-DD/EE/84-1, CERN, Geneva Switzerland (1987) [SPIRES].

[66] Particle Data Group collaboration, C. Amsler et al., *Review of particle physics*, *Phys. Lett.* **B 667** (2008) 1 [SPIRES].

[67] P. Dixon, D. Kant and G. Thompson, *Fragmentation function scaling violations in the Breit frame*, *J. Phys.* **G 25** (1999) 1453 [SPIRES].

[68] P. Deines-Jones et al., *Charged particle production in the Pb + Pb system at* 158 *GeV/c per nucleon*, *Phys. Rev.* **C 62** (2000) 014903 [hep-ex/9912008] [SPIRES].

[69] UA5 collaboration, G.J. Alner et al., *Scaling of pseudorapidity distributions at c.m. energies up to* 0.9 *TeV*, *Z. Phys.* **C 33** (1986) 1 [SPIRES].

[70] B.B. Back et al., *The PHOBOS perspective on discoveries at RHIC*, *Nucl. Phys.* **A 757** (2005) 28 [nucl-ex/0410022] [SPIRES].

[71] A. Bialas and M. Jezabek, *Bremsstrahlung from colour charges as a source of soft particle production in hadronic collisions*, *Phys. Lett.* **B 590** (2004) 233 [hep-ph/0403254] [SPIRES].

[72] T. Tymieniecka and B. Brzozowska, *Limiting fragmentation in e^+e^- annihilation and ep deep inelastic scattering*, *Acta Phys. Polon.* **B 40** (2009) 2175 [SPIRES].

[73] Spin Muon (SMC) collaboration, B. Adeva et al., *Spin asymmetries for events with high p_T hadrons in DIS and an evaluation of the gluon polarization*, *Phys. Rev.* **D 70** (2004) 012002 [hep-ex/0402010] [SPIRES].

JHEP06(2010)009